Molecular dynamics simulations and generalized Lenard-Balescu calculations of electron-ion temperature equilibration in plasmas

Lorin X. Benedict,[1] Michael P. Surh,[1] John I. Castor,[1] Saad A. Khairallah,[1] Heather D. Whitley,[1] David F. Richards,[1] James N. Glosli,[1] Michael S. Murillo,[2] Christian R. Scullard,[1] Paul E. Grabowski,[2] David Michta,[1,3] and Frank R. Graziani[1]

[1]*Lawrence Livermore National Laboratory, Livermore, California 94550, USA*

[2]*Los Alamos National Laboratory, Los Alamos, New Mexico 87545, USA*

[3]*Princeton Plasma Physics Laboratory, Princeton University, Princeton, New Jersey 08543, USA*

(Received 25 July 2012; published 25 October 2012)

We study the problem of electron-ion temperature equilibration in plasmas. We consider pure H at various densities and temperatures and Ar-doped H at temperatures high enough so that the Ar is fully ionized. Two theoretical approaches are used: classical molecular dynamics (MD) with statistical two-body potentials and a generalized Lenard-Balescu (GLB) theory capable of treating multicomponent weakly coupled plasmas. The GLB is used in two modes: (1) with the quantum dielectric response in the random-phase approximation (RPA) together with the pure Coulomb interaction and (2) with the classical ($\hbar \longrightarrow 0$) dielectric response (both with and without local-field corrections) together with the statistical potentials. We find that the MD results are described very well by classical GLB including the statistical potentials and *without* local-field corrections (RPA only); worse agreement is found when static local-field effects are included, in contradiction to the classical pure-Coulomb case with like charges. The results of the various approaches are all in excellent agreement with pure-Coulomb quantum GLB when the temperature is high enough. In addition, we show that classical calculations with statistical potentials derived from the exact quantum two-body density matrix produce results in far better agreement with pure-Coulomb quantum GLB than classical calculations performed with older existing statistical potentials.

DOI: 10.1103/PhysRevE.86.046406 PACS number(s): 52.65.Yy, 52.25.Dg, 52.27.Aj

I. INTRODUCTION

The problem of electron-ion temperature equilibration has enjoyed renewed interest over the past 5 or so years due to the increased excitement resulting from the completion of the National Ignition Facility and a general growing interest in inertial confinement fusion (ICF) [1]. Because of the asymmetric manner in which the α-particle fusion products deposit energy to the electrons and ions, together with the short time scales of the ICF implosion experiment, it is generally believed that significant portions of the thermonuclear burn process will occur in situations where the electrons and ions are out of equilibrium. Since the fusion burn rate depends very sensitively on the ion temperature [2], a precise knowledge of the rate at which the individual species temperatures are driven back to equilibrium (together with an equally precise knowledge of the plasma heating and cooling rates) is desired.

Most if not all integrated simulations of thermonuclear burn [2,3] make use of theoretical equilibration rates of the Landau-Spitzer (LS) variety [4]. In LS theory, an equilibration rate is derived from a Fokker-Plank equation assuming a simple two-body electron-ion collision operator. The result is

$$\frac{1}{\tau_{ei}} = \frac{8\sqrt{2\pi}n_i Z_i^2 e^4}{3m_e m_i c^3}\left[\frac{k_B T_e}{m_e c^2} + \frac{k_B T_i}{m_i c^2}\right]^{-3/2} \ln\lambda_{ei}, \quad (1)$$

where $1/\tau_{ei}$ is the rate at which the electron temperature, T_e, changes given an ion temperature, T_i, according to (assuming a single species of ions),

$$\frac{dT_e}{dt} = \frac{T_i - T_e}{\tau_{ei}}. \quad (2)$$

Electron and ion masses are m_e and m_i, number densities are n_e and n_i, and Z_i is the ion charge. The factor $\ln\lambda_{ei}$ is the so-called Coulomb logarithm, arising from the (divergent) integral of the Rutherford scattering cross section over impact parameter. In a standard treatment the logarithmic divergence is eliminated by setting $\ln\lambda_{ei}$ equal to the logarithm of a ratio of maximum to minimum impact parameters, $\ln(b_{\max}/b_{\min})$. Landau [4] argued that $b_{\max}$ should be chosen to be a Debye screening length, since if the impact parameter is larger than this, an effective two-body collision will not occur. Since he considered classical plasmas, he chose $b_{\min}$ to be the classical turning point distance (now termed the "Landau length"), which for a representative collision between electrons and ions at a temperature T is approximately $b_0 = Ze^2/k_B T$. This assumes that the electron is a pointlike particle which undergoes classical motion. For a quantum plasma, another natural choice for $b_{\min}$ is the thermal de Broglie wavelength, $\lambda_{\rm th}$ [4]. Since $\lambda_{\rm th} \propto 1/\sqrt{T}$ while $b_0 \propto 1/T$, $\lambda_{\rm th}$ is sure to be larger than b_0 for high T, indicating that the close electron-ion collisions will involve a spread-out electron wave packet rather than a classical pointlike electron. If $Z = 1$, $\lambda_{\rm th} > b_0$ for keV plasmas in the fusion-burning regime. Thus, LS theory shows that the short-ranged part of the electron-ion energy transfer can be dominated by quantum diffraction even when the electron occupation numbers are completely Maxwellian.

The LS solution to the electron-ion temperature equilibration problem suffers from two serious deficiencies. (1) It is only applicable for weak plasma coupling, that is, $\Gamma_{ei} = Z_i e^2 n^{1/3}/T \ll 1$ [5]. Indeed, if Γ_{ei} is large, b_0 and/or $\lambda_{\rm th}$ can exceed the screening length, which means that both $\ln\lambda_{ei}$ and the resulting transition rate become negative. (2) As Landau himself admitted, his theory produces predictions of "logarithmic accuracy." If, say, a factor of two or better accuracy is desired (as for the ICF application), LS is likely insufficient *even for weakly coupled plasmas*.

The desire to go beyond LS has prompted numerous researchers to address this problem using other theoretical

and computational means. Those most closely related to the LS treatment involve kinetic and many-body theories in which plasma screening and quantum effects are explicitly taken into account [6]. In this way, the collision integral is computed without the need for *ad hoc*, albeit physically motivated, cutoffs as in the Coulomb logarithm of LS. These include the many-body Green's function approach of Dharma-Wardana and Perrot [7], the kinetic theory + dimensional regularization work of Brown, Preston, and Singleton (BPS) [8], the T-matrix theory of Gericke *et al.* [9], and the quantum Lenard-Balescu treatments of Daligault and Dimonte [10] and Vorberger *et al.* [11]. Though these approaches have produced much in the way of insight, precise numerical predictions of τ_{ei} have been essentially confined to plasmas exhibiting weak electron-ion coupling, particularly for the physically relevant case of opposite charges, since the quantitative inclusion of bound-state effects is still quite challenging at present. Indeed, with the exception of an excellent recent work involving like charges (proton-positron) [10], it is not known how weakly coupled the plasma must be for the above approaches to be predictive. This problem is exacerbated by the complete absence of high-accuracy experimental data of τ_{ei} for plasmas in the fusion-burning regime.

Another approach, capable of including arbitrarily complex many-body correlations for a classical plasma, is molecular dynamics (MD). Since the work of Hansen and McDonald in the 1980s [12], researchers have attempted to compute τ_{ei} in cases where bound states are either unimportant (like-charge or sufficiently high T) or are largely ignored (by positing fixed, time-independent Z_i). The major problem here, of course, is that real plasmas are not classical. As we stated above, for the fusion-burning plasmas which are our interest, quantum diffraction is expected to be essential to include if a reasonable τ_{ei} is to be obtained. In fact, there is an even more basic practical problem: Any plasma composed of opposite charges is *necessarily* quantum mechanical, in that the problem of mutually interacting *classical* electrons and protons is fundamentally ill posed; in a classical simulation, an electron will, through multiparticle energy exchange processes, eventually be forced infinitesimally close to a proton even if they are forbidden to radiate. Indeed, it is the very quantum nature of the electrons which gives rise to the stability of matter [13].

Methods for simulating quantum systems do indeed exist, but none are easily applied to the problem of electron-ion equilibration. Self-consistent electronic structure-based MD, such as that based on various approximations within density functional theory [14], typically invokes Born-Oppenheimer-like assumptions, whereby the electron and ion dynamics are decoupled. This prevents irreversible work from being performed by one subsystem on the other, preventing heat transfer. Quantum Monte Carlo methods have also reached a mature stage [15], but these approaches are generally limited to computing time-independent thermal averages in equilibrium, not nonequlilibrium properties such as energy exchange. True time-dependent Schrödinger dynamics is also coming to fruition, but only for few-body systems [16].

To wit, researchers studying temperature equilibration in plasmas have used classical MD in two varieties: (1) Like-charge MD, in which a truly classical plasma is studied. This has much merit, since for the weakly coupled plasmas (i.e., spatially homogeneous, no bound states) for which LS and related approaches are intended, the like-charge and opposite-charge predictions are exactly the same [4]. Dimonte and Daligault [10,17] have used this approach and have identified a flavor of kinetic theory which reproduces their like-charge MD results strikingly well up to moderate plasma couplings. (2) Opposite-charge MD with two-body statistical potentials (SPs) is the other variety. Here, classical effective potentials are derived which reproduce the correct static structure factors of the quantum plasma; they look essentially like the bare Coulomb interaction at long range and a softened (e.g., finite) potential within the de Broglie wavelength at short range [18–20]. This fixes the opposite-charge classical instability problem, and it is hoped that the softening of the electron-ion potential at short range embodies the salient features of quantum diffraction present for true quantum plasmas. Work in this area includes the original Hansen-McDonald contribution [12], together with more recent work exhibiting far better statistical accuracy: Jeon *et al.* [21], Glosli *et al.* [22], both addressing pure hydrogen, and Benedict *et al.* [23] addressing an idealization of an SF_6 plasma exhibiting weak electron-ion coupling but strong ion-ion coupling.

Both like-charge and opposite-charge MD simulations have verified that LS-type approaches work well for hydrogen plasmas as long as Γ_{ei} is not too large (so, high T and low n), though all have shown that leading-order corrections to LS supplied by, for instance, the BPS theory, are important to include even for $\Gamma_{ei} \sim 0.1$ or less [17,21,22]. For stronger coupling, they clearly show a breakdown of the weak-coupling theories, manifested in the effective Coulomb-log, $\ln \lambda_{ei}^{\text{eff}}$, approaching zero slowly from above as Γ_{ei} is increased [17,22]. Fits to the T-matrix results of Ref. [9] have been shown to reproduce the MD performed with SPs quite nicely for H, in a regime for which Γ_{ei} is fairly large but T is still high enough to prevent bound-state formation [22]. The MD work on the SF_6 plasma exhibited the effects of strong ion-ion coupling but relatively weak electron-ion coupling [23]. In particular, it was seen that the final equilibrated temperature was notably different from what LS (or indeed most of the aforementioned theories) would predict, a result of the screened ions storing potential energy when the ion temperature is low and the ions are strongly correlated. This potential energy contribution to the temperature equilibration problem had been discussed before [24] and has now been modeled in detail by Vorberger *et al.* [11]. It should be stressed that plasmas for which at least some of the ions are strongly coupled are quite probably of the greatest interest at present, since (1) pure H or DT plasmas in the fusion-burning regime ($n \sim 10^{25}$/cc and $T \sim$ a few keV) are probably weakly coupled enough for existing quantum-kinetic treatments to apply, and (2) the admixture of high-Z dopants from the ablator of an ICF capsule into the DT fuel is a very real concern [1].

In this work, we present the results of classical MD simulations, most of which use the SPs, for two systems: pure H, and Ar-doped H for fully ionized Ar ($Z = 18$). For the chosen systems, n varies between 10^{22}/cc and 10^{26}/cc, with the bulk of the simulations concentrated around 10^{25}/cc. Temperatures are between 100 eV and 10s of keV (for the Ar-doped H). These conditions are chosen to coincide with those for DT fusion. While some of the conditions relevant for

fusion include regimes in which the electrons are degenerate [25], we focus largely on those in which the electrons are Maxwellian; this is appropriate for the classical MD studies reported here. The few cases we include that venture into the degenerate regime are considered primarily to afford comparisons between our classical simulations and associated theories (mentioned below).

In addition to presenting MD results for τ_{ei} which are far more accurate than our earlier MD predictions for H [22], we also use a multispecies version of the generalized Lenard-Balescu (GLB) theory, such as that presented in Refs. [10,11], to better understand our MD data. We use the GLB method in two distinct ways: (1) in its quantum variety along with the bare Coulomb potential, and (2) in its classical variety ($\hbar \longrightarrow 0$) with the SPs. By doing (1), we endeavor to learn nature's true answer, at least for the weakly coupled cases where GLB should be accurate. With (2), we address various concerns that arose in our earlier MD work on H [22]. Both (1) and (2) taken together allow us to see the extent to which we should expect classical MD simulations of τ_{ei} to reflect quantum reality. We show that for low-Z plasmas in the fusion-burning regime, classical MD with previously available SPs [18,19] should produce values for τ_{ei} which are within 10%–20% or so of the quantum results. In addition, we use computations of the exact quantum pair density matrix to construct improved SPs for which the agreement is better than this by at least a factor of four, verifying the efficacy of earlier attempts to construct potentials in this manner [20]. While direct comparisons such as these can be done only for weak-coupling (since one is only sure of GLB's validity in such situations), we suspect that some of our conclusions will inform future and ongoing MD studies of strongly coupled quantum plasmas.

II. MOLECULAR DYNAMICS SIMULATIONS

Temperature relaxation simulations are performed with the ddcMD molecular dynamics code [26]. Two-body forces are evaluated with a particle-particle-particle mesh method [27] designed for long-ranged Coulomb and related interactions. Recent optimization of ddcMD allows us to increase the numbers of particles in each simulation by factors of 10^3–10^4 relative to our earlier plasma studies [22,23], with corresponding improvements in statistical uncertainties. Our main goal for these MD studies is to provide guidance for the discrimination between, or development of, theories of electron-ion relaxation for plasmas. In addition, we seek to detect differences in the simulations resulting from the use of different models for the electron-ion interaction. Thus, a fairly high level of statistical accuracy is needed.

The simulations all involve classical many-particle dynamics. In some, we use repulsive $1/r$ potentials, and in others we use quantum SPs [18–20]. The latter are designed to reproduce the equilibrium quantum pair Coulomb correlations by sampling a classical equilibrium distribution with the model potential; they account for quantum mechanical diffraction at short distances in some thermally averaged sense. Both types of potential have been used to compute nonequilibrium plasma properties before [10,12,21–23]. Previous simulations suggest that the temperature relaxation due to Coulomb and SPs differ by 10% or less at moderate coupling for hydrogen [22], so we seek to limit our uncertainties to much less than this. Because our MD code scales well, we use large systems (1 024 000 particles for H) to minimize statistical errors instead of many independent, small replicas. In a few cases, we compare the results from statistically uncorrelated replicas to quantify the uncertainties for these large simulations. In the following discussion, we describe the details of our hydrogen simulations, though similar approaches are used for the Ar-doped H plasma simulations we also present below.

We prepare nonequilibrium, two-temperature hydrogen plasmas so as to minimize initial transient behavior during the temperature relaxation runs. The particles are started in a perfect ionic lattice in the CsCl structure. This artificial placement ensures that long wavelength charge fluctuations are initially zero. The longest wavelength acoustic modes relax slowly for large systems, and it is preferable to begin with a well-characterized density not far from the expected thermal distribution. In contrast, our prior use (in small systems) of a random mixture at quasiuniform density [22,23] can introduce spurious, athermal charge density fluctuations that must then be annealed from the system. No attempt has been made to seed the CsCl structure with density fluctuations appropriate to the temperature and compressibility of the system, although this could be done in the future. The initial particle velocities are drawn randomly from separate Maxwell-Boltzmann distributions. We add separate, weak Langevin thermostats to the electrons and protons,

$$m_\alpha \dot{v} dt = -\frac{m_\alpha v}{\tau_\alpha} dt + \sqrt{\frac{2kTm_\alpha}{\tau_\alpha}} d\xi, \tag{3}$$

during the MD sample preparation. Here, $d\xi$ is white noise and $\alpha \in \{e,i\}$ for electrons and ions. Typically, the species-dependent velocity decay time, τ_α, is adjusted to exceed the plasmon (for electrons) or ion acoustic wave (for ions) period, or density oscillations are overdamped and their evolution can be delayed. In order to quickly approach a stationary state, we initially scale the proton masses to $m_p \simeq m_e$. An MD simulation is performed over multiple oscillation periods until the distribution of amplitudes for the longest-wavelength modes appears to be stationary. The disparate species temperatures equilibrate rapidly for $m_p \simeq m_e$; this causes departures from the two-temperature profile and alters the nonequilibrium pair correlations. Afterwards, the proton masses are rescaled logarithmically towards their physical values, and all particle velocities are rescaled to recover the desired species' temperatures. The system is then annealed for a similar interval as before. The subsequent temperature equilibration is slower due to the increased adiabatic separation of ions and electrons, and the final configuration is closer to the desired two-temperature limit. In particular, the density fluctuation spectrum and total potential energy more closely approximate that for the nonequilibrium temperature relaxation problem. The sequence (mass-scaling, velocity-scaling, and thermostated MD) is repeated three times, until the final proton mass is obtained.

The physical electron mass is used in all simulations, but the proton mass has been taken for the most part to be $1824m_e$ here, rather than its true physical mass ($\sim 1836m_e$). This is simply because of an error in defining the proton mass in the

MD code which was not caught until later; the closeness of the chosen value to the true value allows us to assert that the physical value of any computed temperature relaxation time can be recovered by appealing to Eq. (1) and scaling the reported relaxation times (computed with $m_p = 1824 m_e$) by the factor 1.0066.

The as-prepared system has quasi-Maxwell-Boltzmann distributions near the desired temperatures, and density fluctuations that approximate a stationary, but nonequilibrium distribution. In some cases, independent samples are obtained by repeating this procedure, starting from the stationary configuration just described. The initial mass scaling, $m_p \simeq m_e$, quickly reaches a state that is uncorrelated to the starting configuration.

Temperature relaxation rates are obtained by microcanonical MD simulations of the as-prepared nonequilibrium systems. Simulation durations range from $<1\%$ to substantial fractions of τ_{ei}, and $\Delta T = T_e(t) - T_p(t)$ relaxes by as little as 0.1% for weak-coupling cases and up to 50% for strong coupling. We perform a nonlinear least squares fit of a relaxation function $F(C(t - t_0))$ to $\Delta T(t)$ over the entire simulation interval, in terms of a rate C and time offset t_0. The relaxation time $\tau_{ei}^{-1} = C d\ln(F)/dt$. Different analytic results for $F(t)$ have been used in the past [10]; here the fitting function is a numerical solution to

$$\frac{dF}{dt} = -\left(F_e + \frac{F_p}{1824}\right)^{-3/2} \ln\left(F_e^{1/2}\right) F, \tag{4}$$

where $F_e = F/2 + T_\infty$ represents the fit electron temperature in a LS-like expression, $F_p = -F/2 + T_\infty$, and T_∞ is some average $(T_e + T_p)/2$, an estimate for the asymptotic, equilibrium temperature in the weak-coupling limit, and m_p/m_e is here assumed to be 1824. This is adjusted accordingly in the few cases where a reduced proton mass is used in the temperature relaxation simulations. Equation (4) includes leading deviations from constant linear relaxation. However, it does not account for strong-coupling cases where equilibration $T_{eq} \neq T_\infty$ due to changing potential energy contributions [23,24]. An example of the raw MD data, together with the aforementioned fit, appears in Fig. 1 for a hydrogen plasma at $n = 10^{25}$/cc (discussed in Sec. IV A).

The numerical uncertainty in τ_{ei} cannot be estimated from the fit to a single short simulation because fluctuations in relative temperature occur over times characteristic of τ_{ei}. A lower bound to the error can be obtained by considering the equilibrium situation. When two systems are in thermal equilibrium with an external bath, their internal energies fluctuate:

$$\overline{(\delta E)^2} = \overline{E^2} - (\overline{E})^2 = k_B T^2 C_v \tag{5}$$

(Ref. [28], 6.5.5. and 7.2.13). The heat capacity for the kinetic energy of the electrons or protons is just the ideal gas $C_v = \frac{3}{2} N k_B$. If the bath is removed, the temperatures of the two species will still fluctuate, each serving as a (finite) bath for the other. This implies

$$\overline{\left(\tfrac{3}{2} N k_B \delta T\right)^2} = \tfrac{3}{2} N (k_B T)^2 \tag{6}$$

and a relative uncertainty in the temperature of $\delta T/T \simeq (3N)^{-1/2}$, about 0.1% for the simulations considered here. The autocorrelation time for these fluctuations is related to

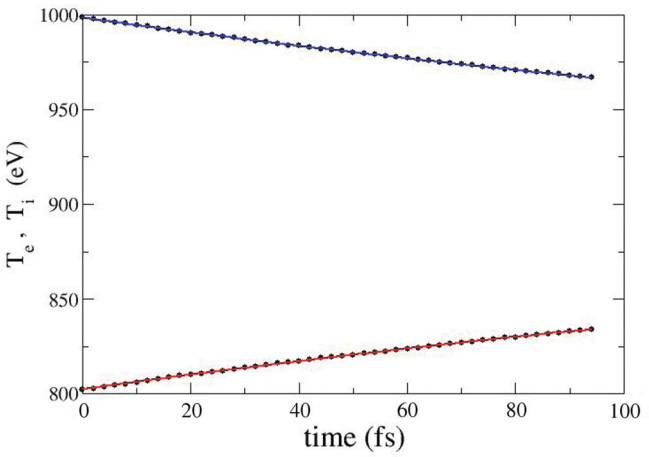

FIG. 1. (Color online) Raw data (black dots) for the simulation of temperature equilibration in a hydrogen plasma with $n = 10^{25}$/cc and initial electron and proton temperatures of 1000 and 800 eV, respectively. Dunn-Broyles + Deutch SPs were used in the MD simulation. Solid blue and red curves show the fit to the data which is used to extract the value of τ_{ei}.

τ_{ei}. For example, an equilibrium simulation of hydrogen at $\rho = 10^{22}$/cc $T_e = T_p = 30$ eV, using the Dunn-Broyles and Deutsch potentials [18,19] for the interparticle interactions predicts $\tau_{ei} \simeq 1450$ fs. This is obtained from the first 70 fs of the $\langle \Delta T(t) \Delta T(0) \rangle$ autocorrelation function from a 400-fs simulation. In comparison, two independent, 150-fs, *non*-equilibrium simulations with $T_p = 60$ eV, $T_e = 30$ eV give $\tau_{ei} \simeq 1545$ fs from the direct numerical fit to ΔT (see Table I). If multiple short (e.g., duration $0.01\tau_{ei}$), statistically independent, equilibrium simulations are performed, the slope $d\Delta T/dt$ will average to zero, with an uncertainty of order $\delta T/\tau_{ei}$ or 0.1%. A comparable error will apply to the $d\Delta T/dt$ and the rate constant derived from short nonequilibrium temperature relaxation runs. Finally, the nonequilibrium temperature relaxation runs are compatible with these estimates. The residual or difference between the simulated $T_i - T_e$ and the fitted function fluctuates with an amplitude that is consistent with the near equilibrium conditions of the simulation.

There are additional contributions to the uncertainty between independent simulations. The isothermal sample preparation described above gives an ensemble of systems with different internal energies; $\frac{T_e + T_i}{2}$ may differ at the 0.1% level, resulting in slightly different expected τ_{ei} throughout the simulations. However, an explicit sampling of independent calculations with 5×10^5 hydrogen suggest that τ_{ei} differs by 1%–2%. Larger errors occur because kinetic energy is also exchanged with the potential energy of the system. The heat capacity due to the potential energy is proportionately small in the weak coupling limit, but the relevant correlation time constant can be shorter than τ_{ei}. Thus, the influence of potential energy fluctuations is magnified by a short simulation. There may also be residual transient relaxations from the sample preparation. In practice, our demonstrated numerical accuracy is sufficient to distinguish between some theories of electron-ion equilibration in interesting regimes, and at least some different models for electron-proton (ep) interactions, regardless of the sources of error.

TABLE I. MD simulation results for τ_{ei} (in fs) for hydrogen at $n = 10^{22}$/cc. The electron temperatures are the values used in computing the numerical relaxation rate; they lie within the range of temperatures spanned by the simulation. Proton temperatures are calculated from T_∞ and so vary slightly for different sample realizations. The target temperature is shown here. The relaxation columns are in fs and are labeled by potential type (all simulations used a Deutsch form for the Pauli term) and particle types (*ep*, electron-proton; *pp*, positron/proton). For all but the last τ_{ei} reported ($\Gamma_{ei} = 0.005$ case), two independent MD runs were performed; the results here indicate the average.

T_p (eV)	T_e (eV)	Γ_{ei}	Dunn-Broyles (*ep*)	Dunn-Broyles (*pp*)	Coulomb (*pp*)
59.5	30.5	0.167	1517	1542	1333
199.5	100.5	0.050	5708	5204	4295
599.4	300.5	0.017	21 833	18 939	15 522
1996	1002	0.005	95 226		

MD plasma simulations are most challenging in the weak coupling limit; relaxation times are large here, so long simulations are required. The high thermal velocities also demand small time steps to resolve trajectories for small impact parameter collisions. The $1/r$ Coulomb potential poses the most stringent time step requirements; the use of SPs to include quantum diffraction effects greatly ameliorates this trend. Numerical errors manifest most prominently as a failure of energy conservation, but it is essential to note that good energy conservation is by no means a sufficient condition to ensure that the temperature equilibration rate is converged. We maintain a high degree of energy conservation, typically parts in 10^3–10^4 over a simulation in which temperature differences may relax by anywhere from 10% to 0.1%. Explicit checks that τ_{ei} itself is converged with respect to dt are complicated by the computational difficulties of running multiple simulations with sufficiently large numbers of particles and for the required long run times. One such convergence test appears in Fig. 2. For each dt chosen, multiple statistically independent $2-T$ replicas are run long enough to obtain τ_{ei}. It is apparent in this case that for the numbers of particles used (5×10^5 electrons and protons), the statistical spread in the resulting relaxation times limits the assessment of time step convergence. This problem only gets worse as T is increased at fixed particle density. Nevertheless, we find that for the SPs we use in most of our study, and for hydrogen densities of 10^{25}/cc (this isochore is discussed extensively below), sufficiently small time steps range from 10^{-5} fs for $T \sim$ few hundred eV to 10^{-7} fs for $T \sim$ many keV. For this reason, we are not able to study extremely weakly coupled cases with this approach.

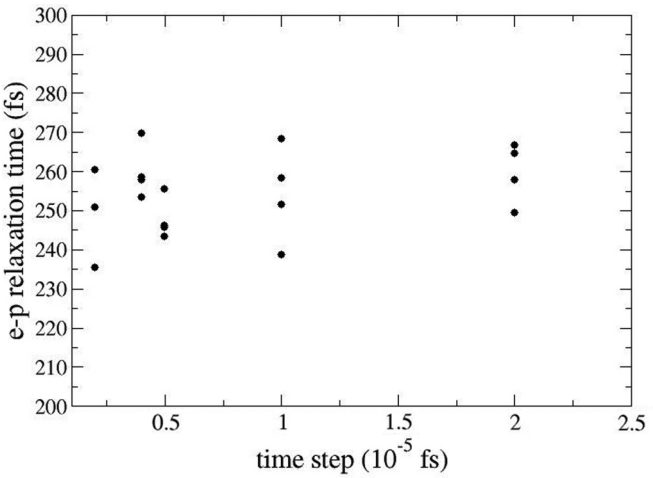

FIG. 2. Values of τ_{ei} extracted from MD runs for a hydrogen plasma ($n = 10^{25}$/cc, $T_e = 1000$ eV, $T_p = 800$ eV, Dunn-Broyles + Deutch potentials) as a function of the MD time step. The multiple points for each time step indicate statistically independent replicas.

Finally, we consider four models for electron-ion scattering. The classical Coulomb potential is only considered for like-sign charges (a proton-positron gas) in order to eliminate (singular) classical bound states. Three SPs are also compared; they (when attractive) include bound states in generating the correct equilibrium pair correlations $g(r)$. Most simulations are performed with the Dunn and Broyles diffractive correction to the Coulomb potential [18], along with a Deutsch term for the Pauli exclusion for electrons [19],

$$U_{\alpha\beta}(r,T) = \frac{Z_\alpha Z_\beta e^2}{r}\left[1 - \exp\left(\frac{-2\pi r}{\Lambda_{\alpha\beta}}\right)\right] + k_B T \ln(2) \exp\left(\frac{-4\pi r^2}{\ln(2)\Lambda_{\alpha\beta}^2}\right)\delta_{\alpha e}\delta_{\beta e}, \quad (7)$$

where $\Lambda_{\alpha\beta} = \sqrt{2\pi\hbar^2/\mu_{\alpha\beta}k_B T}$ and $\mu_{\alpha\beta} = m_\alpha m_\beta/(m_\alpha + m_\beta)$. This is the form used in the early Hansen and McDonald [12] paper on MD of temperature relaxation. We consider both opposite- and like-sign charges for these potentials. We also examine a new diffractive correction based on calculations of the exact quantum pair density matrix at a given temperature. These potentials, which we discuss directly below, are related to the Kelbg form, so we also compare temperature relaxation using the Kelbg potential [20].

A. Statistical potentials based on the exact pair density matrix: Modified Kelbg

In order to treat electrons as classical particles in an MD simulation, a variety of quantum SPs have been developed. Their use in the study of plasmas was pioneered by Hansen and co-workers [12,29–32]. The effects of quantum diffraction, interference, and the Pauli exclusion principle are incorporated in these potentials in a thermally averaged sense. In this work, we utilize these existing SPs, in addition to new potentials derived from the diagonal part of the exact Coulomb pair density matrix and fit to a modified form of the Kelbg potential

[20,33,34]. This treatment and its limitations are presented in greater detail in Refs. [35,36].

A statistical potential for a pair of particles can be defined from the nonideal part of the exact pair density matrix, $\rho_2(\mathbf{r}_{ij},\mathbf{r}_{ij};\beta)$,

$$U^C(r_{ij},\beta) = -\frac{1}{\beta}\ln\left[\frac{\rho_2(\mathbf{r}_{ij},\mathbf{r}_{ij};\beta)}{\rho_F(\mathbf{r}_{ij},\mathbf{r}_{ij};\beta)}\right], \tag{8}$$

where

$$\rho_F(\mathbf{r}_{ij},\mathbf{r}_{ij};\beta) = (2\pi\beta\hbar^2/\mu_{ij})^{-3/2}\exp[-\mu_{ij}|\mathbf{r}_{ij}|^2/2\hbar^2\beta]$$

is the free particle density matrix, $\beta \equiv (k_B T)^{-1}$, and μ_{ij} is the reduced mass of the interacting pair of particles. Our computation of ρ_2 for electron-electron and electron-proton cases is discussed elsewhere [35,36]. We fit our results for the statistical potential with the modified Kelbg form for a pair of particles with indices i and j [33],

$$U^C(r_{ij},\beta) = \frac{Z_i Z_j}{r_{ij}}e^2\left[1 - e^{-(\frac{r_{ij}}{\lambda_{ij}})^2}\right] + \sqrt{\pi}\frac{Z_i Z_j}{\lambda_{ij}\gamma_{ij}}e^2\left(1 - \mathrm{erf}\left[\gamma_{ij}\frac{r_{ij}}{\lambda_{ij}}\right]\right), \tag{9}$$

where we treat λ_{ij} and γ_{ij} as temperature-dependent fitting parameters. At very high temperatures, in the limit of weak coupling, λ_{ij} is equal to the thermal de Broglie wavelength, $\lambda_{ij}^2 = \frac{\hbar^2\beta}{2\mu_{ij}}$, and $\gamma_{ij} = 1$, and we therefore recover the original Kelbg potential [20]. As the temperature is reduced and the coupling increases, these parameters deviate from the weakly coupled values. We examine the behavior of the fitting parameters over a wide range of temperatures in order to derive the following expressions for electron-electron (ee) and ep interactions [36]:

$$\begin{aligned}
\lambda_{ee} &= \sqrt{\frac{\hbar^2\beta}{m_e}}\left(1 + \frac{0.005}{\sqrt{T}}\right),\\
\gamma_{ee} &= 1 + \frac{0.0321}{T^{0.4664}},\\
\lambda_{ep} &= \sqrt{\frac{\hbar^2\beta}{2m_p}}\left(1 - \frac{0.002}{T}\right),\\
\gamma_{ep} &= 1 - \frac{0.06}{\sqrt{T}},
\end{aligned} \tag{10}$$

where T is expressed in Hartrees.

For the ee interaction, we add an additional term to $U^C(r_{ij},\beta)$ to account for the effect of Fermi statistics. Here, we use the same form as adopted by Hansen and co-workers [12,29–32], which was originally suggested by Deutsch, Gombert, and Minoo [19,37,38],

$$U_{ee}(r_{ij},\beta) = U^C(r_{ij},\beta) + \beta^{-1}\ln(2)\exp\left(-[\pi\ln(2)]^{-1}r^2/\Lambda_H^2\right), \tag{11}$$

where $\Lambda_H = \hbar/\sqrt{\pi m_e k_B T}$. We stress that a two-body term such as this cannot account for strong electron degeneracy; it is meant here to incorporate corrections to classical statistics that appear as the temperature is lowered slightly below the regime where purely classical statistics should apply.

III. GENERALIZED LENARD-BALESCU THEORY

A. Theory

In order to understand our MD results, we use the GLB theory as presented in Ref. [10], which is itself based partly on the intellectual constructs of Ichimaru [39]. In their treatment, the time rates of change of the species temperatures, due to Ohmic heating of one species by the others, are related to ensemble averages of products of density fluctuations. Assuming spatial homogeneity of the particle densities, the expressions for dT/dt may be written as double integrals over k and ω space. We consider arbitrary numbers of species here, a straightforward generalization of the work of Refs. [10,40],

$$\frac{dT_\alpha}{dt} = \frac{1}{\pi^2 n_\alpha \Omega^2}\left[\sum_{\beta\neq\alpha}\sum_{\mathbf{k}}\int_0^\infty d\omega\omega v_{\alpha\beta}(\mathbf{k}) \times \mathrm{Im}\langle\delta n_\alpha(\mathbf{k},\omega)\delta n_\beta(-\mathbf{k},-\omega)\rangle\right], \tag{12}$$

where $v_{\alpha\beta}(\mathbf{k})$ is the Fourier transform of the two-body interaction between particles of species α and particles of species β. The δn_α are the density fluctuations in the presence of the interparticle interactions. The ensemble average of their products is related to the exact dielectric response, or polarizability tensor [39]. Care must be taken when defining the precise meaning of the ensemble average involved here; the time-scale for this averaging must be long enough to identify individual-species equilibrium temperatures (provided that they make sense), but short compared to the interspecies equilibration time that we aim to compute [10,39]. This is possible as long as the ion mass is significantly greater than the electron mass, for instance, but must necessarily be called into question when the equilibrating species have more similar masses.

In order to connect this average to quantities which are calculable, we assume a linear responselike relation between the interacting density fluctuations, and the *spontaneous*, or ideal gas, fluctuations, $\delta n_\alpha^{(s)}$ [10,39],

$$\delta n_\alpha = \delta n_\alpha^{(s)} + \chi_\alpha^0\sum_\beta v_{\alpha\beta}[1 - G_{\alpha\beta}]\delta n_\beta, \tag{13}$$

where it is understood that the argument of each quantity is (k,ω). The $\delta n_\alpha^{(s)}$ are the density fluctuations *in the absence* of interactions. Note that β can equal α in this sum. This equation describes the manner in which the density fluctuations of one species (with free-particle linear polarizability, χ^0) are induced by the fluctuations of all the other species. The factors, G's, are the local field corrections (LFCs); if all the G's are set equal to zero, this is just the random-phase approximation (RPA) for multiple species. As discussed in the work of Ref. [10], it is essential to include the LFC in cases where the Landau length, b_0, exceeds the thermal de Broglie wavelength of the lighter-mass species. RPA ($G = 0$) works well when the reverse is true, as well as in cases where one species is highly degenerate. This is discussed more in what follows.

Equation (13) is a matrix equation in the species indices (α,β) which must be solved for the δn_α in terms of the $\delta n_\alpha^{(s)}$. Once this is done, the ensemble average in Eq. (12), $\langle\delta n_\alpha\delta n_\beta\rangle$, can be rewritten in terms of ideal gas (i.e., free

particle) averages, $\langle \delta n_\alpha^{(s)} \delta n_\beta^{(s)} \rangle$. These are well known and can be readily computed for any density and temperature [39]. Then the right-hand side of Eq. (12) can be evaluated. We write the formal solution to Eq. (13) as

$$\delta n_\alpha = -\sum_\beta B_{\alpha\beta} \delta n_\beta^{(s)}, \tag{14}$$

where $B_{\alpha\beta}$ is the matrix inverse of the matrix, $A_{\alpha\beta}$, defined by

$$A_{\alpha\beta} = \chi_\alpha^0 v_{\alpha\beta}[1 - G_{\alpha\beta}] - \delta_{\alpha,\beta}. \tag{15}$$

Then we have

$$\langle \delta n_\alpha(+) \delta n_\beta(-) \rangle = \sum_\mu \sum_\nu B_{\alpha\mu}(+) B_{\beta\nu}(-) \times \left\langle \delta n_\mu^{(s)}(+) \delta n_\nu^{(s)}(-) \right\rangle, \tag{16}$$

where (+) indicates $(\mathbf{k},\omega)$, and (−) indicates $(-\mathbf{k},-\omega)$. The ensemble averages of products of free-particle density fluctuations are related to the (free-particle) dynamic structure factors through [10,39]

$$\left\langle \delta n_\mu^{(s)}(\mathbf{k},\omega) \delta n_\nu^{(s)}(-\mathbf{k},\omega') \right\rangle = (2\pi)^2 \delta_{\mu,\nu} \delta(\omega + \omega') \times \Omega S_{\mu\mu}^0(\mathbf{k},\omega), \tag{17}$$

and the structure factors are related back to the independent-particle polarizabilities through the fluctuation-dissipation theorem [39],

$$S_{\mu\mu}^0(+) = -\frac{\hbar}{2\pi} N\left(\frac{\hbar\omega}{2k_B T_\mu}\right) \mathrm{Im}\chi_\mu^0(+), \tag{18}$$

where $N(x) = \coth(x)$. The final result for the time rate of change of the species temperature is then obtained by inserting Eqs. (16)–(18) into Eq. (12), obtaining

$$\frac{dT_\alpha}{dt} = -\frac{\hbar}{3\pi^3 n_\alpha} \int_0^\infty k^2 dk \int_0^\infty \omega d\omega \sum_{\beta\neq\alpha} v_{\alpha\beta}(k) \mathrm{Im} \left\{ \sum_\mu \left[N\left(\frac{\hbar\omega}{2k_B T_\mu}\right) B_{\alpha\mu}(+) B_{\beta\mu}(-) \mathrm{Im}\chi_\mu^0(+) \right] \right\}. \tag{19}$$

For the case of just two species, electrons and ions, this expression can be simplified to [10,24]

$$\frac{dT_i}{dt} = -\frac{\hbar}{3\pi^3 n_\alpha} \int_0^\infty k^2 dk \int_0^\infty \omega d\omega \left[\frac{v_{ei}(k)}{D(k,\omega)}\right]^2 [1 - G_{ei}(k,\omega)] \left[N\left(\frac{\hbar\omega}{2k_B T_i}\right) - N\left(\frac{\hbar\omega}{2k_B T_e}\right) \right] \mathrm{Im}\chi_e^0(k,\omega) \mathrm{Im}\chi_i^0(k,\omega), \tag{20}$$

once the matrix inverse of Eq. (15) is explicitly evaluated to obtain the $B_{\alpha\beta}$. The $D(k,\omega)$ involves the v's, χ^0's, and G's and essentially represents the plasma dielectric function [10,24,39],

$$D = \left[1 - v_{ee}(1 - G_{ee})\chi_e^0\right]\left[1 - v_{ii}(1 - G_{ii})\chi_i^0\right] - v_{ei}^2 (1 - G_{ei})(1 - G_{ie})\chi_e^0 \chi_i^0. \tag{21}$$

Note that dT_i/dt is proportional to the square of the electron-ion interaction and is also proportional to the imaginary parts of both electron and ion free-particle susceptibilities. As discussed in Refs. [7,10,24], because the ion plasma frequency is much lower than the electron plasma frequency (owing to the large mass difference), $\mathrm{Im}\chi_i^0$ is peaked at very low ω, and this allows one to use the f-sum rule to evaluate the remaining factors at $\omega \longrightarrow 0$. Though this is a fine approximation for H [10], we choose not to make this replacement in this work, since some of the cases which interest us have multiple ion species and/or involve scaled ion masses (see the Ar-doped H cases discussed later).

It is instructive to see how Eq. (20) relates back to an LS-type result. Though we refer the reader to the more detailed discussion of this in Ref. [10], we highlight the salient points here, in which we consider electrons and protons interacting via the Coulomb interaction: Once the ω integral has been performed, we are left with an integral over k. From the above discussion, the resulting integrand will involve the various factors evaluated near $\omega = 0$. For small k, the integrand will be forced to zero by the dielectric function, D, which becomes large for k smaller than the screening (Debye) wave vector. This then provides the "$b_{\max}$" of LS. For large k, $\mathrm{Im}\chi_e^0(k,\omega \longrightarrow 0)$ is proportional to $\exp(-\lambda_{\mathrm{th}}^2 k^2)$ [41] for a nondegenerate quantum plasma, so the k integrand will be forced to zero when k is larger than the de Broglie wave vector, $1/\lambda_{\mathrm{th}}$. This gives rise to the choice of $b_{\min} = \lambda_{\mathrm{th}}$ in LS. If the electrons are degenerate, $\chi_e^0(k,\omega \longrightarrow 0)$ will go to zero rapidly beyond $k \sim 2k_{\mathrm{Fermi}}$ [10,24,41]. For a *classical* plasma, $\mathrm{Im}\chi_e^0(k,\omega \longrightarrow 0)$ approaches a constant, $-n_e/k_B T_e$, independent of k; in this case, the large-k cutoff can only arise from the $1 - G_{ei}$ factor. For like-charge plasmas this factor has been shown to go to zero right when k approaches the inverse Landau length [10], hence providing the impetus for the identification, $b_{\min} = b_0$. Thus, the expression of Eq. (20) and its multi-ion generalization in Eq. (19) represent theories devoid of the logarithmic divergences that plague LS. Plasma screening mitigates the low-momentum (large b) divergence, while quantum diffraction and/or two-body correlations (embodied in $G_{\alpha\beta}$) eliminate the high-momentum (small b) divergence; no *ad hoc* cutoffs are needed [10].

There are three types of quantities which are required in order to compute dT_α/dt with Eq. (19): the Fourier transforms of the two-body interactions, $v_{\alpha\beta}(k)$, the free-particle susceptibilities, $\chi_\alpha^0(k,\omega)$, and the LFCs, $G_{\alpha\beta}(k,\omega)$. Not much is known about the ω dependence of the $G_{\alpha\beta}$. Though there are methods that purport to obtain it [39,42], the various approximations involved have not been thoroughly tested for real plasmas. We follow the approach of Ref. [10] and restrict our attention to static LFCs, $G_{\alpha\beta}(k)$, for which various methods apply; we

discuss $G_{\alpha\beta}$ more below. For the two-body interactions, $v_{\alpha\beta}(k)$, we use either the Coulomb interaction, $4\pi Z_\alpha Z_\beta e^2/k^2$, or the Fourier transform of a SP. The free-particle susceptibilities, $\chi^0_\alpha(k,\omega)$, are computed from the expression [39,41]

$$\chi^0_\alpha(k,\omega) = \lim_{\eta\to 0^+}\left[2\sum_{\mathbf{k}'}\frac{f_\alpha(\mathbf{k}'+\mathbf{k})-f_\alpha(\mathbf{k}')}{\frac{\hbar^2(\mathbf{k}'+\mathbf{k})^2}{2m_\alpha}-\frac{\hbar^2k'^2}{2m_\alpha}-\hbar\omega+i\eta}\right], \quad (22)$$

where $f_\alpha(\mathbf{k})$ is the Fermi-Dirac occupancy for particles of energy $\hbar^2k^2/2m_\alpha$ at a temperature of T_α. For quantum particles, the imaginary part of χ_0 has an analytic expression as a function of density and temperature while the real part of this quantity for electrons has been tabulated and fit for all n and T by Dandrea, Ashcroft, and Carlsson [43]. We use their fit, which is very accurate for both degenerate and nondegenerate electrons. We note that the dependence on mass in Eq. (22) allows us to scale their result to use it for quantum ions as well, provided that the proper (n,T)-dependent chemical potential for the ions is used in the resulting expressions.

As we mentioned earlier, we use the GLB in two modes: quantum with the bare Coulomb interaction (QC) and classical ($\hbar \longrightarrow 0$) with the SPs (CS). For QC, we apply the above prescription exactly as stated and set $v_{\alpha\beta}(k) = 4\pi Z_\alpha Z_\beta e^2/k^2$. For CS, we not only choose the Fourier transform of a SP for $v_{\alpha\beta}(k)$, but we also take the $\hbar \longrightarrow 0$ limit in two distinct places. The first is in the free-particle polarizabilities, $\chi^0_\alpha(k,\omega)$. Here, we make use of the relation [10]

$$\lim_{\hbar\to 0}\left[\mathrm{Im}\chi^0_e(k,\omega)\right] = -\frac{\sqrt{\pi}n_e}{k_BT_e}Ye^{-Y^2}, \quad (23)$$

where $Y = \sqrt{m_e/2k_BT_e}(\omega/k)$, and the corresponding expressions for $\mathrm{Im}\chi^0_i(k,\omega)$. The real part is then obtained by appealing to the so-called plasma dispersion function (also known as Dawson's function),

$$\mathrm{Re}\epsilon(\tilde{k},\tilde{\omega}) = 1+\frac{1}{\tilde{k}^2}-\sqrt{\frac{\pi}{2}}\frac{\tilde{\omega}}{\tilde{k}^3}e^{-\frac{\tilde{\omega}^2}{2\tilde{k}^2}}\mathrm{erfi}\left(\frac{\tilde{\omega}}{\sqrt{2}\tilde{k}}\right), \quad (24)$$

where χ^0_e is related to ϵ via $\epsilon = 1-(4\pi e^2/k^2)\chi^0_e$. In the above equation, $\mathrm{erfi}(x) \equiv -i\mathrm{erf}(ix)$, $\tilde{k} \equiv k/k_D$, and $\tilde{\omega} \equiv \omega/\omega_p$, where k_D is the Debye wave vector and ω_p is the plasma frequency. The second place where the $\hbar \longrightarrow 0$ limit is taken is in the N-function appearing in Eq. (19). Here we simply set $N(x) = 1/x$ for the classical case [10]. It should be mentioned that this second change is almost immaterial for low-Z systems as long as the ions are chosen to have their physical masses; since the ion plasma frequency is far lower than the electron plasma frequency, most of the important contributions to the integrand of Eq. (19) are for $\omega \approx 0$, which also leads to $N(\hbar\omega/2k_BT) \longrightarrow 2k_BT/\hbar\omega$. Thus, the major changes when studying the classical case are the appearance of the SP in $v_{\alpha\beta}(k)$ and the use of the classical electron polarizability.

Note that for QC, $v_{\alpha\beta}(k)$ decreases slowly with k, as $1/k^2$, while $\chi^0_e(k,\omega \longrightarrow 0)$ dies off exponentially for k greater than $1/\lambda_{\mathrm{th}}$, providing the large-k convergence of the integral. For CS, $v_{\alpha\beta}(k)$ dies off quickly above $1/\lambda_{\mathrm{th}}$, while $\chi^0_e(k,\omega \longrightarrow 0)$ goes to a constant. In both cases, the k integral converges at large k, but for *different* reasons. This illustrates how the effect of quantum diffraction, arising from the χ^0_e in the quantum calculation, gets inserted into the SPs in the classical calculation. It is this classical GLB calculation which is analogous to our MD. While this insertion is strictly unfounded, we see below that the differences between τ_{ei} computed with QC and τ_{ei} computed with CS get rather small as the fusion-burning regime is approached (see the Appendix for a detailed discussion of this).

To go beyond the RPA in the calculation of the plasma dielectric response [embedded in the $\langle\delta n_\alpha\delta n_\beta\rangle$ of Eq. (12) and the $B_{\alpha\mu}B_{\beta\mu}$ of Eq. (19)], we make use of static LFCs, $G_{\alpha\beta}(k)$. Since these are a direct result of physics beyond the RPA [cf. Eq. (13)], they must be derived by comparing some manifestation of RPA density-density response to an analogous quantity determined in an ostensibly less approximate way. We choose to focus on the static two-body radial distribution functions, $g_{\alpha\beta}(r)$, the conditional probability of finding a particle of species β between r and $r+dr$ away from a particle of species α. The radial distribution functions are related to the static structure factors by Fourier transformation [39],

$$g_{\alpha\beta}(r) = 1+\frac{1}{\sqrt{n_\alpha n_\beta}}\sum_{\mathbf{k}}[S_{\alpha\beta}(k)-\delta_{\alpha\beta}]e^{i\mathbf{k}\cdot\mathbf{r}}, \quad (25)$$

and the resulting inverse transformation,

$$S_{\alpha\beta}(k) = \delta_{\alpha\beta}+\sqrt{n_\alpha n_\beta}\int d^3\mathbf{r}e^{-i\mathbf{k}\cdot\mathbf{r}}[g_{\alpha\beta}(r)-1], \quad (26)$$

where $S_{\alpha\beta}(k) = \frac{1}{\sqrt{n_\alpha n_\beta}}\int_{-\infty}^{\infty}d\omega S_{\alpha\beta}(k,\omega)$. From the fluctuation-dissipation theorem, we can relate the structure factors to the polarizabilities [39],

$$S_{\alpha\beta}(\mathbf{k},\omega) = -\frac{\hbar}{2\pi}\coth\left(\frac{\hbar\omega}{2k_BT}\right)\mathrm{Im}\chi_{\alpha\beta}(\mathbf{k},\omega), \quad (27)$$

where we assume for simplicity that the whole system is in thermal equilibrium at a temperature, T. In this way, we can compute the $g^{\mathrm{RPA}}_{\alpha\beta}(r)$ from $\chi^{\mathrm{RPA}}_{\alpha\beta}(k)$ and compare them to the "true" $g_{\alpha\beta}(r)$ produced some more accurate way, say from MD, or from some less approximate theory than RPA.

In order to relate this comparison to the $G_{\alpha\beta}$, we start from their definition in Eq. (13), and extract the interacting polarizability, $\chi_{\alpha\beta}$: Upon the application of an external potential, Φ_β, acting on species β, a resulting density fluctuation, δn_α, will be induced in species α [39],

$$\delta n_\alpha = \sum_\beta \chi_{\alpha\beta}\Phi_\beta = \chi^0_\alpha\left[\Phi_\alpha+\sum_\beta v_{\alpha\beta}(1-G_{\alpha\beta})\delta n_\beta\right]. \quad (28)$$

The expression in brackets on the right-hand side is the total potential felt by the α-species particles, which is composed of an external piece (Φ_α) and an induced potential which involves the LFCs. This relates the interacting polarizability, $\chi_{\alpha\beta}$, which responds to the *external* potential to the free-particle polarizability, χ^0_α, which responds to the *total* potential. Like Eq. (13), this is a matrix equation in the species indices. Solving for the LFCs gives

$$1-G_{\alpha\beta} = \frac{1}{v_{\alpha\beta}}\left[\frac{1}{\chi^0_\alpha}\delta_{\alpha\beta}-[\chi^{-1}]_{\alpha\beta}\right], \quad (29)$$

where $[\chi^{-1}]$ denotes the matrix inverse of the $\chi_{\alpha\beta}$ matrix. The prescription is then as follows: Determine the $g_{\alpha\beta}(r)$ using

MD or some other means. Compute $S_{\alpha\beta}(k)$ from them using Eq. (26). Solve Eq. (27) to obtain $\chi_{\alpha\beta}(k)$ from $S_{\alpha\beta}(k)$ (see below), and then invert the χ matrix to obtain the $G_{\alpha\beta}(k)$ from Eq. (29).

There are three additional points regarding our scheme for obtaining the LFCs which must be mentioned. (1) Equation (27) relates $S_{\alpha\beta}$ to $\mathrm{Im}\chi_{\alpha\beta}$, rather than to both the real and imaginary parts of $\chi_{\alpha\beta}$. We require both the real and the imaginary parts, yet in order to obtain $\mathrm{Re}\chi_{\alpha\beta}(k)$ from $\mathrm{Im}\chi_{\alpha\beta}$, we would have to use the Kramers-Kronig transform, which itself requires knowledge of $\mathrm{Im}\chi_{\alpha\beta}(k,\omega)$ [or $S_{\alpha\beta}(k,\omega)$] for *all* ω. This dynamical information is very difficult to obtain for a quantum many-particle system [39,42]. Thus, we choose to compute the LFCs for our classical cases (CSs) only. For classical particles, the static limit of Eq. (27) is simply written as [39]

$$S_{\alpha\beta}(k) = -\frac{k_B T}{\sqrt{n_\alpha n_\beta}}\chi_{\alpha\beta}(k,\omega=0), \tag{30}$$

so both real and imaginary parts of $\chi_{\alpha\beta}(k)$ are obtained once the static structure factors are known. (2) We use a combination of two methods to determine the $g_{\alpha\beta}(r)$ for our various CS cases: MD, and the hypernetted chain approximation (HNC) [30]. Both methods constitute improvements upon RPA; both use the $v_{\alpha\beta}(k)$ as input, which we take to be our various forms of SPs for the opposite-charge plasmas we study, and the bare Coulomb interaction for the few like-charge cases we consider. (3) Equation (27) assumes thermal equilibrium, yet our interest is in situations for which T_α differs from T_β. We believe this to be of negligible importance as long as T_α and T_β are not too dissimilar. For most of our cases this is satisfied, and even when T_e and T_i differ by a lot, equilibrium and nonequilibrium MD results for $g_{\alpha\beta}(r)$ are in very good accord (see below). Thus, we carry out the prescription of Eqs. (16)–(20) for plasmas *in equilibrium*, and then apply the resulting LFCs to the associated out-of-equilibrium problems.

1. Hypernetted-chain evaluation of static LFCs

There is a close connection between the LFCs obtained from Eq. (29) and the direct correlation function that has a central role in the hypernetted-chain method.

If we let the total correlation functions $h_{ij}(r)$ be defined by $h_{ij} \equiv g_{ij} - 1$, then the direct correlation functions $c_{ij}(r)$ are introduced with the quite general Ornstein-Zernicke (OZ) relation [30],

$$h_{ij}(\mathbf{r}) = c_{ij}(\mathbf{r}) + \sum_k n_k \int d^3\mathbf{r}'\, h_{ik}(\mathbf{r}-\mathbf{r}')c_{kj}(\mathbf{r}'). \tag{31}$$

The HNC closes this system of equations with the expression for $h_{ij}(r)$

$$h_{ij}(r) = \exp[h_{ij}(r) - c_{ij}(r) - \beta U_{ij}(r)] - 1, \tag{32}$$

in which $U_{ij}(r)$ is the pair potential for the pair (i,j) and which could be either the Coulomb interaction or an effective potential with quantum diffraction and Pauli corrections [44]. We note that the HNC method is limited to the CS; indeed, the OZ relation has a modified form when the electrons are treated quantum mechanically [44,45]. For particular choices of density, temperature, particle densities n_k, and the potentials $U_{ij}(r)$, Eqs. (31) and (32) may be solved for h_{ij} and c_{ij} by a nonlinear iteration [46,47].

In Fourier space the OZ relation takes the form

$$\tilde{h}_{ij}(\mathbf{k}) = \tilde{c}_{ij}(\mathbf{k}) + \sum_k n_k \tilde{h}_{ik}(\mathbf{k})\tilde{c}_{kj}(\mathbf{k}). \tag{33}$$

The earlier expression (26) for the static structure functions $S_{ij}(k)$ can be written

$$S_{ij}(k) = \delta_{ij} + \sqrt{n_i n_j}\,\tilde{h}_{ij}(k). \tag{34}$$

It is convenient to write h_{ij}, c_{ij}, and S_{ij} in matrix form: $H = (h_{ij})$ and so forth. We introduce a diagonal matrix d of particle densities with

$$d_{ij} = \delta_{ij} n_i, \tag{35}$$

and denote by $d^{1/2}$ the diagonal matrix with diagonal values $\sqrt{n_i}$. Then the OZ relation becomes

$$\tilde{H} = \tilde{C} + \tilde{C}d\tilde{H}, \tag{36}$$

of which the solution for $\tilde{H}$ is

$$\tilde{H} = (I - \tilde{C}d)^{-1}\tilde{C}, \tag{37}$$

where I is the unit matrix.

The matrix form of the defining relation [Eq. (34)] for S is

$$S = I + d^{1/2}\tilde{H}d^{1/2}. \tag{38}$$

With a little manipulation it can be shown that

$$S = I + d^{1/2}(I - \tilde{C}d)^{-1}\tilde{C}d^{1/2} = (I - d^{1/2}\tilde{C}d^{1/2})^{-1}. \tag{39}$$

We make contact between the matrix S and the density-density response function matrix χ by expressing Eq. (30) as

$$\beta S(k) = -d^{-1/2}\chi(k)d^{-1/2}, \tag{40}$$

and, since in the CS $\chi^0_\alpha = -\beta n_\alpha$, Eq. (29) becomes

$$\begin{aligned} 1 - G_{ij} &= \frac{1}{\beta\tilde{v}_{ij}}[-d^{-1} + d^{-1/2}S^{-1}d^{-1/2}]_{ij} \\ &= -\frac{1}{\beta v_{ij}}\{d^{-1/2}[I - S^{-1}]d^{-1/2}\}_{ij} \\ &= -\frac{1}{\beta v_{ij}}\tilde{c}_{ij}. \end{aligned} \tag{41}$$

Since the quantities $\tilde{c}_{ij}(k)$ are by-products of the HNC calculation, and $\tilde{v}_{ij}(k)$ is identified with the effective potential $\tilde{U}_{ij}(k)$, the LFCs are found immediately when the HNC calculation is done.

It may be noted that the matrix A in Eq. (15) is just

$$A = d\tilde{c} - I = -d^{1/2}S^{-1}d^{-1/2}, \tag{42}$$

so

$$\det(A) = -\frac{1}{\det(S)} = -\det(I - d^{1/2}\tilde{C}d^{1/2}) \tag{43}$$

is the negative of the discriminant $D(k,0)$, related to the static dielectric function, as appearing in Eq. (21) for the two-component case.

B. Numerical details

In order to compute dT_α/dt for the various species using Eq. (19), we must identify a suitable (k,ω) grid over which to compute the double integral numerically. The challenge here is that $\mathrm{Im}\chi_i^0(k,\omega)$ is peaked at very low ω in the neighborhood of the ion plasma frequency, $\omega_i = \sqrt{4\pi Z_i^2 e^2 n_i/m_i}$, while $\mathrm{Im}\chi_e^0(k,\omega)$ is peaked at the generally much higher electron plasma frequency, $\omega_e = \sqrt{4\pi e^2 n_e/m_e}$. We use an exponential grid in ω such that $\omega_{\min} = 10^{-7} \times \sqrt{2T/m_e}/r_s$, and $\omega_{\max} = 10^5 \times \sqrt{2T/m_e}/r_s$. This large value of $\omega_{\max}$ ensures that for suitably large T_e, the broadening of the electron plasmon peak is well represented. Also, since the plasmon disperses with k, this large $\omega_{\max}$ also ensures that the plasmon peak is contained for the largest values of k we choose (recall that the plasmon energy increases with increasing k [39]).

For the k mesh, we also use an exponential grid, though this is certainly less crucial than for the ω integral. The $k_{\min}$ is chosen to be $10^{-3}/r_S$, where r_S is the Wigner-Seitz radius, while $k_{\max}$ is chosen to be $10^4/r_S$. These choices are appropriate for densities ranging from 10^{22}/cc to 10^{26}/cc and temperatures between 1 eV and 20 keV, since $k_{\min}$ will be comfortably below $1/\lambda_{\mathrm{Debye}}$, and $k_{\max}$ will be large enough to encompass the range over which $\mathrm{Im}\chi_e^0(k)$ decreases to zero well above $k = 1/\lambda_{\mathrm{th}}$.

For all of our calculations using Eq. (19), we use a modified rectangular-rule integration in which the logarithm of the independent variable is used in defining the differential. For the k integral, for example, we take $u = \ln k$ and write

$$\int F(k)dk = \int kF(k)\frac{dk}{k} = \int kF(k)du \approx \sum_i k_i F(k_i)[\ln k_{i+1} - \ln k_i]. \quad (44)$$

An identical expression is used for the ω integral. The number of integration points we use is $N_k = 1801$ and $N_\omega = 1201$. We determined that these numerical parameters are sufficient for accurately computing the dT_α/dt by converging the results with respect to $k_{\min}$, $k_{\max}$, $\omega_{\min}$, $\omega_{\max}$, N_k, N_ω, as well as by requiring that the f-sum rule be *simultaneously* satisfied for both electrons *and* ions,

$$-\int_0^\infty \omega d\omega \left(\frac{4\pi Z_{e,i}^2 e^2}{k^2}\right) \mathrm{Im}\chi_{e,i}^0(k,\omega) = \frac{\pi {\omega_{e,i}}^2}{2}. \quad (45)$$

With the aforementioned parameter choices, electron and ion f-sum rules are satisfied to within one part in 10^5 using a *single* ω mesh, and for all relevant k [note that the right-hand side in Eq. (45) is independent of k].

For the HNC calculations of the static LFCs, we iteratively solve the simultaneous system Eqs. (31) and (32) with a nonlinear adaptation of the GMRES method [48] which accelerates the solution. Some of the HNC applications in this paper need quite a large dynamic range in r and also in k in order to describe the full variation of $1 - G_{ij}$. The coding uses equally spaced meshes to allow efficient Fourier transforms, the most costly operations involved. The present calculations used $2^{17} = 131\,072$ points in r and k.

IV. RESULTS AND DISCUSSIONS

A. Hydrogen

Relaxation times, τ_{ei}, determined from the MD simulations are presented in the rightmost columns of Tables I–IV, under headings indicating the types of interparticle potentials used. They are the results of the MD simulations, where the proton mass had been fixed at 1824 times the (physical) electron mass. As discussed above in Sec. II, this was an oversight; all reported MD relaxation times have been scaled up by a factor of 1.0066 to account for this. The reported temperatures are selected to avoid extrapolation of T_e outside the simulation interval. The instantaneous T_p's are then calculated from T_∞ and the fitting function of Eq. (4); they differ slightly between independent samples. The results for τ_{ei} are not sensitive to T_∞, whether taken as the average of temperatures at $t = 0$ or t_{final}, or an average over the simulation. Here we use the instantaneous temperatures at $t = 0$ to compute T_∞. In some cases, we perform multiple uncorrelated MD simulations for a given set of conditions in order to assess variability. Note that for essentially all our studied cases, these run-to-run variations in τ_{ei} are significantly larger than the error estimates of our determination of the initial slope, dT_e/dt, for any *single* run.

Table I shows a collection of MD results for H at a density of 10^{22}/cc. Note first that as the electron and ion temperatures increase, τ_{ei} increases. This is to be expected from any theory of temperature equilibration, such as LS [4]. Weaker electron-ion coupling, here indicated in the third column, gives rise to slower electron-ion relaxation. Second, note that opposite-charge and like-charge results with the same potential (Dunn-Broyles) give similar results. This is also expected, particularly for the fairly weakly coupled ($\Gamma_{ei} \sim 0.01$–0.2) cases here, as motivated again by LS. We stress, however, that the equilibration times of Table I are the result of running the MD simulations for a time less than $0.01\tau_{ei}$, owing to the difficulty of simulating such weakly coupled cases (as discussed in Sec. II above). As such, detailed quantitative trends cannot be gleaned from these data, as evidenced by

TABLE II. MD simulation results for τ_{ei} (in fs) for the hydrogen isochore, $n = 10^{25}$/cc. The actual initial species temperatures are shown here. GLB (and/or LS) theory shows that the values of τ_{ei} are essentially the same as they would have been if these initial temperatures had been exactly equal to the target temperatures (say, $T_p = 80$ eV and $T_e = 100$ eV, rather than $T_p = 83$ eV and $T_e = 98$ eV), owing to the closeness of actual and target initial temperatures. The errors in τ_{ei} reported are the result of computing the standard deviation for several statistically independent MD runs for the same conditions. For the value in which no error is reported, only a single MD run was performed.

T_p (eV)	T_e (eV)	Γ_{ei}	Dunn-Broyles
83	98	0.500	56.02 ± 0.82
180	195	0.250	67.23
203	245	0.200	77.86 ± 0.34
414	488	0.100	127.59 ± 0.88
805	995	0.050	249.29 ± 5.3
1608	1995	0.025	553.63 ± 26
4004	5000	0.010	1602.51 ± 71

TABLE III. MD simulation results for τ_{ei} (in fs) for hydrogen with various forms of SPs.

n (H/cc)	T_p (eV)	T_e (eV)	Γ_{ei}	Dunn-Broyles	Kelbg	Modified Kelbg
1.25×10^{24}	200	248	0.100	298.67	262.82	257.75
10^{25}	400	500	0.100	126.05	114.97	113.39
10^{25}	800	998	0.050	232.99	224.91	212.39
8×10^{25}	1600	1993	0.050	101.22	99.68	88.16

the apparent divergence of opposite-charge and like-charge results as Γ_{ei} is decreased, in contrast to expectation. Finally, we note that the like-charge τ_{ei} results with the pure Coulomb interaction are smaller than those obtained with the statistical potential for the same conditions, and these differences between the τ_{ei} increase as the temperature is increased. This is because the electron thermal de Broglie wavelength is significantly larger than the Landau length at high T (discussed above in Sec. I); the statistical potential is softened within the de Broglie wavelength while the Coulomb interaction is not, so the effective $b_{\min}$ in the $\ln \lambda_{ei}$ of Eq. (1) is smaller for pure Coulomb than for the Dunn-Broyles treatment.

Since we have invoked LS in understanding the gross features of the results pertaining to Table I, it is natural to ask the following: Do these MD results agree quantitatively with LS (and related approaches)? The first two cases in Table I were studied earlier by some of us in Ref. [22], albeit with much smaller system sizes which led to lower accuracy. In Fig. 2 of that work, the effective $\ln \lambda_{ei}$ (which is proportional to $1/\tau_{ei}$) extracted from MD results using the Dunn-Broyles potential is shown along with the predictions of LS and BPS [8] and a fit to the results of Ref. [9]. The MD equilibration rates for these cases were 60% or so lower than those predicted by the theories, though this was somewhat obscured by the fact that our error bars were large enough to render this difference nearly unresolved. Our more converged results for these cases present equilibration rates which are a bit higher than those of Ref. [22] but are still substantially lower than LS and BPS. The LS and BPS predictions for τ_{ei} for $T_e = 30$ eV and $T_p = 60$ eV are 1207 and 1103 fs, respectively, roughly 25%–33% lower than our MD results for the electron-proton systems using the Dunn-Broyles potential. At the higher temperatures, $T_e =$ 100 eV and $T_p = 200$ eV, we get 3982 and 4431 fs. These are 25%–36% lower than the MD results. Some of this discrepancy likely results from a lack of convergence due to the challenges of performing the MD at such weak plasma couplings (short simulation times, etc.). However, the reason for much of this discrepancy is that these theories pertain to energy transfer between quantum particles mediated by the pure Coulomb interaction. The MD τ_{ei}, in contrast, are the result of classical dynamics with a modified, statistical potential.

To demonstrate that this assertion is correct, we use the GLB theory to calculate the τ_{ei} for these cases in two different ways, as discussed above in Sec. III A. Local-field effects are neglected for now ($G_{ij} = 0$); we include them later. First, we use the quantum prescription (QC). This produces $\tau_{ei}(T_p = 60 \text{ eV}) = 1108$ fs, and $\tau_{ei}(T_p = 200 \text{ eV}) = 4466$ fs, nearly equivalent to the quantum BPS predictions [22]. Next, we use the $\hbar \to 0$ classical prescription and the Dunn-Broyles potential (CS), which yields $\tau_{ei}(T_p = 60 \text{ eV}) = 1276$ fs, and $\tau_{ei}(T_p = 200 \text{ eV}) = 4922$ fs, somewhat closer to our MD results. This strongly suggests that the underprediction of the electron-ion temperature equilibration rate for the higher-T weak coupling cases, as compared with the theories and shown in Fig. 2 of Ref. [22], is partly due to the use of classical dynamics and the Dunn-Broyles potential. We show below that for higher temperature cases, the discrepancy between our classical MD with Dunn-Broyles potentials and weak-coupling theories which assume quantum dynamics and the pure Coulomb interaction are almost entirely accounted for in this way.

How accurate should we expect classical MD with a statistical potential to be in predicting τ_{ei} for hydrogen? Can this approach still be of use in, for instance, differentiating between candidate theories? We address this by studying temperature relaxation for hydrogen at different temperatures along the $n = 1.0 \times 10^{25}$/cc isochore. This is a density very relevant for ICF, and moreover, the increased Γ_{ei} (relative to the $n = 10^{22}$/cc cases) allows us to obtain more accurate MD results. We consider electron temperatures between 100 eV and 20 keV, and for each case, we take $T_p = 0.8T_e$. For all these temperatures, $\lambda_{\text{th}} > b_0$, so quantum diffraction should govern the lower length scale in the Coulomb logarithm of LS.

Figure 3 shows the results of various calculations of the initial slope in the proton temperature, dT_p/dt, as a function of $T_e(t = 0)$ [again, with $T_p(t = 0) = 0.8T_e(t = 0)$]. The gross features of these curves (e.g., the maxima at $T_e \sim 1$ keV) are due to the fact that $dT_p/dt \propto (T_e - T_p) \propto T_e$, together with the dependencies of λ_{th}, λ_{Debye}, and the prefactor of Eq. (1) on T_e, as per LS. The red points are the results of GLB in the QC mode, with LFCs set equal to zero (see below). This should be the true answer for hydrogen at the highest T_e's, since Γ_{ei} is quite small there. Though we do not display them in this figure, these QC-GLB results are essentially identical to those of the quantum limit of BPS [8]. The magenta squares show the MD results with the Dunn-Broyles SPs. The associated τ_{ei} values are displayed numerically in Table II. In the plot, the values for the individual statistically independent MD runs are shown (several for each T_e); these are the values which contribute to

TABLE IV. Relaxation rates (in eV/fs) for scaled-mass ($\alpha =$ 0.01) Ar-doped H, in which Dunn-Broyles + Deutch potentials are used. Species densities are $n_p = 10^{25}$/cc, $n_{\text{Ar}} = 10^{24}$/cc, and $n_e = 2.8 \times 10^{25}$/cc. Z_{Ar} is fixed at +18. Both MD and GLB results are shown.

	MD	QC-GLB	CS-GLB ($G = 0$)	CS-GLB (G)
dT_{Ar}/dt	−0.0885	−0.1709	−0.0896	−0.0854
dT_p/dt	−0.0138	−0.0224	−0.0122	−0.0116
dT_e/dt	0.011	0.0141	0.0076	0.0084

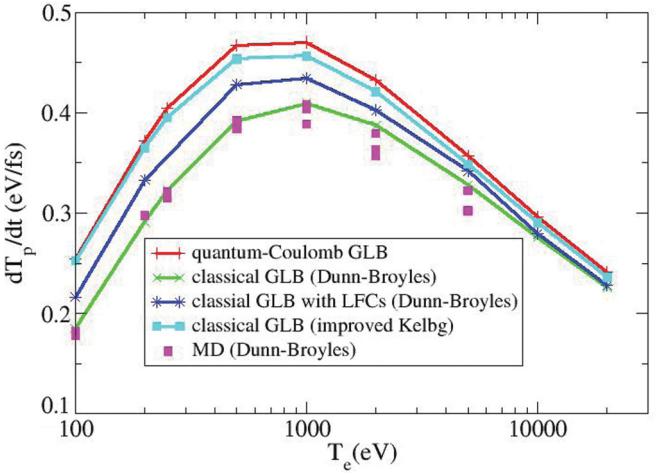

FIG. 3. (Color online) Values of the initial ($t = 0$) dT_p/dt for H along an isochore at a density, $n = 10^{25}$/cc, for which $T_p(t = 0) = 0.8T_e(t = 0)$. Results of GLB calculations of different types (see text) and MD results are shown.

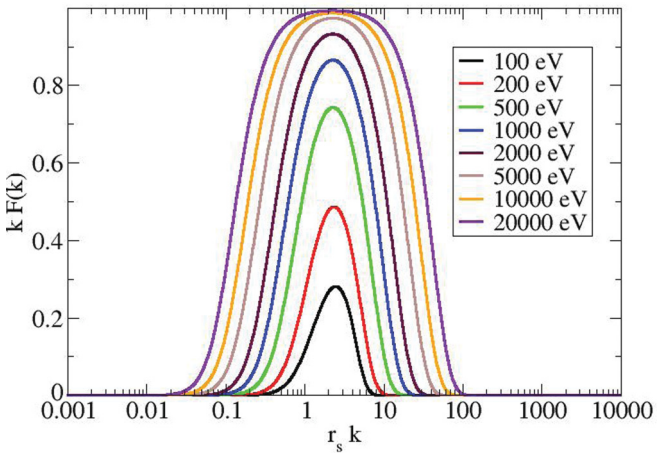

FIG. 4. (Color online) $kF(k)$ (see text for definition) vs kr_S for various τ_{ei} H simulations along the $n = 10^{25}$/cc isochore. These are the results of GLB calculations in the quantum-Coulomb (QC) mode. LFCs (G_{ij}) are set to zero.

the errors reported in the associated table. As for $n = 10^{22}$/cc, the MD equilibration rates lie quite below the QC-GLB results, though they approach them as T_e is increased [49]. The green symbols represent the results of GLB in the CS mode (LFCs = 0), where the same Dunn-Broyles SPs were used. They are in very good agreement with the MD results. This suggests that the error incurred by using classical MD with the Dunn-Broyles potential can be largely quantified and understood by examining the differences between QC-GLB and CS-GLB. These distinctions were discussed in Sec. III A: quantum versus classical short-wavelength dielectric response and Coulomb versus softened SPs. Note that for $T =$ a few keV, temperature relaxation from classical MD with the Dunn-Broyles potential should be well within 10% of the quantum result.

It is important to note that at these keV temperatures, the use of the statistical potential in MD simulations is crucial: Since $\lambda_{\rm th}$ is much larger than b_0, the magnitude of the relaxation is sensitively dependent on the softening of the potential at short range. The fact that the MD and QC-GLB agree reasonably well means that this softening is accounting for the salient features of true quantum diffraction, though in a necessarily approximate way. We also add that high accuracy in predictions of τ_{ei} with classical MD and these SPs is by no means guaranteed, since the potentials are, at best, only constrained to reproduce *static* properties of the quantum plasma. The roughly 10%–15% or so difference between our Dunn-Broyles MD and QC-GLB is therefore encouraging, particularly since the ICF community is not in need of predictions of τ_{ei} which are much better than this.

Before continuing further in our analysis of MD results of τ_{ei} for hydrogen, we briefly discuss some features of our GLB predictions that shed light on the physics of temperature equilibration. Much of this expands upon the discussion in Sec. III A and a similar discussion in Ref. [10]. In order to make an explicit connection between our GLB results and LS, we consider the k integrand of an effective Coulomb logarithm, $F(k)$, defined by

$$\int_0^\infty F(k)dk = \frac{3m_e m_i c^2}{8\sqrt{2\pi}n_e Z_i^2 e^4}\left[\frac{k_B T_e}{m_e c^2}+\frac{k_B T_i}{m_i c^2}\right]^{3/2}\frac{dT_i/dt}{(T_e - T_i)}, \tag{46}$$

where dT_i/dt is given by the expression of Eq. (19) (for $\alpha = i$; we consider just two species here). $F(k)$ is defined so that its integral over k equals $\ln\lambda_{ei}$ in cases where the more general GLB result of Eq. (19) reduces to LS [Eqs. (1) and (2)]. These cases are characterized by having Maxwellian electron and ion distributions, an ion mass that greatly exceeds the electron mass, and species temperatures which are not too dissimilar. Figure 4 shows a plot of QC-GLB results for $kF(k)$ versus $r_S k$ for all the cases of our $n = 10^{25}$/cc isochore. As T_e is increased, $kF(k) \longrightarrow 1$ for intermediate values of k. LS corresponds to $F(k) \equiv 1/k$, together with the constraint that the integral over k is taken to be $\int_{k_{\rm min}}^{k_{\rm max}} F(k)dk$, where $k_{\rm min} = 1/b_{\rm max}$ and $k_{\rm max} = 1/b_{\rm min}$. The QC-GLB $F(k)$ possess maxima at small k and then goes quickly to zero as $k \longrightarrow 0$, due to the sharp increase in the plasma dielectric function at long wavelength for $k < k_{\rm Debye}$. For large k, $F(k)$ goes to zero *very gradually* as k is increased well beyond $1/\lambda_{\rm th}$, due to quantum diffraction arising from the $\mathrm{Im}\chi_e^0$ factor in Eq. (20). In this way, one sees the sense in which LS can be viewed as an approximation to GLB. The approximation is the most reasonable at the weakest couplings since here, $F(k) \sim 1/k$ for *intermediate* values of k, yet even in such cases, it is only perfectly accurate *if one happens to choose* $b_{\rm min}$ and $b_{\rm max}$ in such a way that $\int_{1/b_{\rm max}}^{1/b_{\rm min}} dk/k \equiv \int_{k_{\rm min}}^{k_{\rm max}} dk/k = \int_0^\infty F(k)dk$.

Figure 5 shows both QC-GLB and CS-GLB results for $kF(k)$ for the case: $n = 10^{25}$/cc, $T_e = 1$ keV, $T_p = 0.8$ keV, where the Dunn-Broyles potentials are used for $v_{\alpha\beta}(k)$ in the CS-GLB calculation. The differences between the quantum pure-Coulomb theory and the classical theory with the softened statistical potential can here be seen in a momentum-resolved way. Note that the small-k parts of the two $F(k)$ are identical. This is expected, since the long-range parts of the statistical and Coulomb potentials are the same, and the resulting screening at

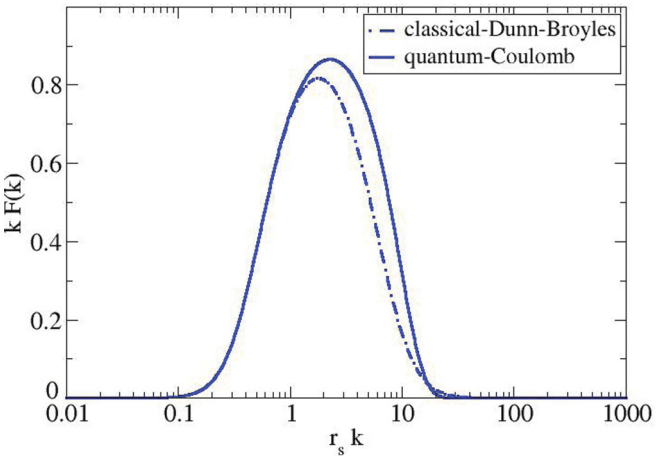

FIG. 5. (Color online) $kF(k)$ vs kr_S for $T_e = 1$ keV and $T_p = 0.8$ keV for H. Both QC and CS GLB results are shown. The statistical potential is of the Dunn-Broyles variety. LFCs (G_{ij}) are set to zero.

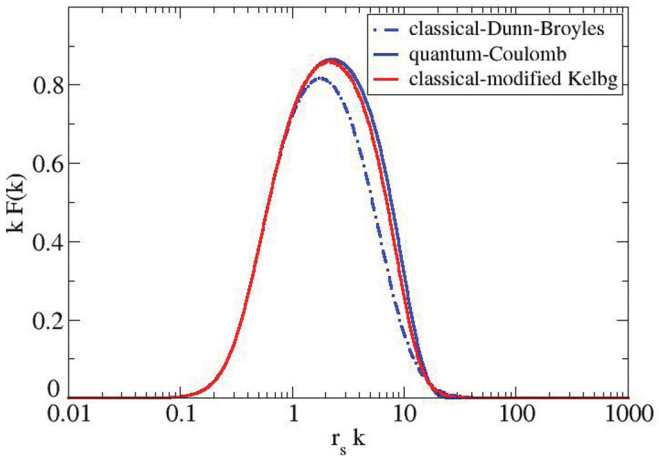

FIG. 6. (Color online) $kF(k)$ vs kr_S for $T_e = 1$ keV and $T_p = 0.8$ keV for H. Both QC and CS GLB results are shown. Statistical potentials of both the Dunn-Broyles and modified-Kelbg varieties are considered. LFCs (G_{ij}) are set to zero.

large distances is therefore also the same. The intermediate and large-k behavior is notably different, however. As discussed in Sec. III A, these differences are the combined result of the short-ranged softening in the statistical potential, and the drastic difference between classical and quantum electron dielectric response. The comparison shown in Fig. 5 suggests that it should be possible to *optimize* $v_{ei}^{SP}(k)$ to require that CS-GLB produces *exactly* the same $F(k)$ as QC-GLB. Indeed, we would simply need to iterate the $\hbar \longrightarrow 0$ version of Eq. (20) to convergence in comparison with the QC result. Here, that would involve increasing $v_{ei}^{SP}(k)$ somewhat at large k. Though this approach for designing an effective potential to be used in classical simulations by optimizing agreement with a *time-dependent* property of a quantum system is certainly reasonable, we choose not to do this here. Time-dependent quantum phenomena are not known precisely for many-body systems such as a plasma, except at very weak coupling. Though $T = 1$ keV and $n = 10^{25}$/cc in pure H may indeed constitute weak enough coupling for this to work, we prefer to base any improvements to existing SPs on static, equilibrium properties, since these are known essentially for all plasma couplings (see the end of the Appendix for a discussion of a statistical potential constrained to reproduce the QC result for temperature equilibration at weak coupling).

To this end, we adopt the modified Kelbg (MK) potentials introduced in Sec. II A. Referring back to Fig. 3, the sky-blue symbols are the results of CS-GLB performed with the MK SPs. These dT_e/dt are significantly closer to the QC-GLB predictions than they are to the CS-GLB results with the Dunn-Broyles potentials. Just as for Dunn-Broyles, the MK results asymptote to the pure-Coulomb quantum answers at high T_e. Our GLB studies strongly suggest that classical MD to determine temperature equilibration should be a factor of 4 or so more accurate if MK rather than Dunn-Broyles potentials are used. The results shown in Table III show differences between Dunn-Broyles and modified Kelbg simulations, which are of the proper magnitudes. Figure 6 shows the $kF(k)$ for the same case as in Fig. 5, but with the MK CS-GLB result overlayed. The difference between the Dunn-Broyles and MK F's is notable; this results in the difference between green and sky-blue points at $T_e = 1$ keV seen in Fig. 3. In addition, $F(k)$ from the MK CS-GLB is almost indistinguishable from the $F(k)$ of QC-GLB *even though no attempt was made to fit directly to the quantum GLB result*. Better agreement with static properties is enough to generate a statistical potential far better suited for temperature equilibration simulations, at least for the weak-coupling cases such as this one, where QC-GLB should be accurate.

We mention in passing that for all the cases studied so far, MD results for τ_{ei} produced with our *modified* Kelbg potentials and results obtained for the identical cases with the original Kelbg potentials [20] are the same within our statistics (compare the last two columns of Table III). This means that for hydrogen in the fusion-burning regime, the Kelbg form is generally the form of choice for calculations of τ_{ei}. We remind the reader, however, that results obtained with the Dunn-Broyles/Deutch prescription are *qualitatively* similar, and asymptote to those of Kelbg (and modified Kelbg) at sufficiently high T.

Up to now, our discussion of results has involved GLB calculations with no LFCs (i.e., $G_{ij} = 0$). As we mentioned in Sec. III A, we do not attempt to estimate LFCs in the quantum cases [42]; this we save for a subsequent investigation. It is still of interest, however, to include LFCs in our classical GLB studies, aimed at directly reproducing our MD results with this or that potential. We consider *static* LFCs only, $G_{ij}(k,\omega) \equiv G_{ij}(k)$, as recommended in Ref. [10], and compute them with HNC, as described in detail in Secs. III A and III A 1. The results are easy to summarize: In all cases studied, the relaxation rates are larger if static LFCs are included and seem to be in *worse* agreement with MD, given our present understanding of the statistical and finite-size errors in those simulations. Figure 3 shows this clearly for the $n = 10^{25}$/cc isochore. The dark-blue points are the CS-GLB results with the Dunn-Broyles potential and including the $G_{ij}(k)$ as calculated by HNC with this potential. Again, the predictions of all the approaches converge at high T_e, but the discrepancies below a few keV are systematic and large. Though not shown in the figure, CS-GLB results with HNC-derived $G_{ij}(k)$ for the MK

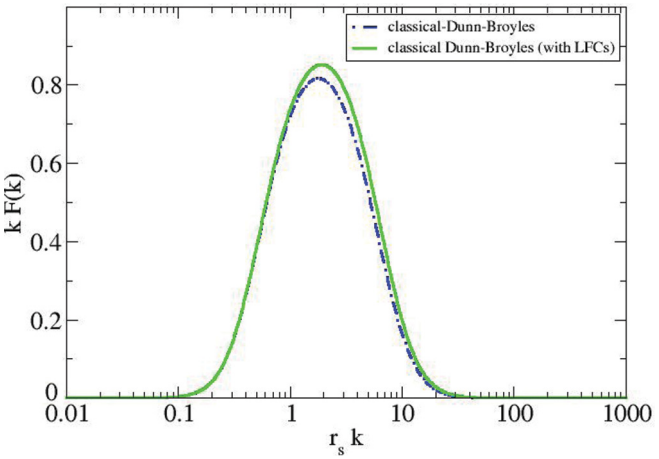

FIG. 7. (Color online) $kF(k)$ vs kr_S with and without LFCs for $T_e = 1$ keV and $T_p = 0.8$ keV for H. Classical-statistical potential GLB results are shown. The statistical potential is of the Dunn-Broyles variety.

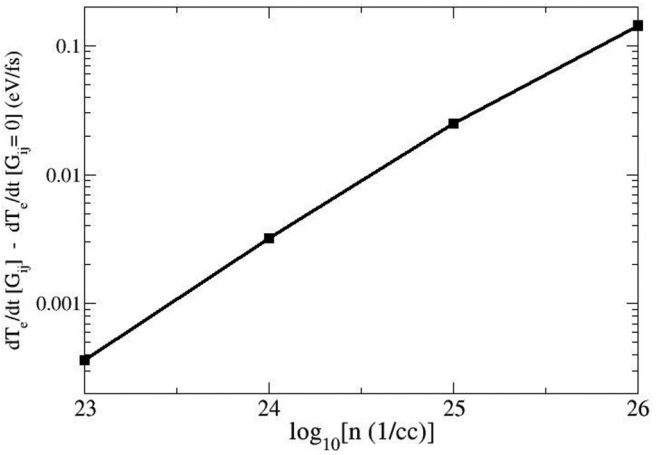

FIG. 9. Differences (including LFC vs not including LFCs) between absolute values of dT_e/dt for H along the $T_e = 1$ keV isotherm, where $T_p = 0.8$ keV. The results are those of CS GLB with the Dunn-Broyles potential.

potential also overpredict dT_e/dt relative to MD with those potentials, while the $G_{ij}(k) = 0$ GLB results with the MK potentials seem to be in better agreement.

Figure 7 shows the $kF(k)$ as computed with CS-GLB and the Dunn-Broyles potential for the same case as shown in Figs. 5 and 6, for both $G_{ij}(k) = 0$ and $G_{ij}(k) \neq 0$. The $F(k)$ including LFCs is quite a bit larger in magnitude than the no-LFC $F(k)$, even for rather small k. This is because the $1 - G_{ei}(k)$ appearing in Eq. (20) has quite a bit of structure at low k and asymptotes to a value significantly greater than 1 at larger k, as shown in Fig. 8. It is this behavior of the LFCs that causes the equilibration rates to be larger than the no-LFCs results, as we have seen in Fig. 3.

We emphasize that the exercise of identifying a theoretical approach which reproduces the results of classical MD is somewhat separate from that of constructing a theory for nature's true hydrogen plasma. Though we ultimately aim for the latter, it seems appropriate to first understand the classical cases, since here, MD with sufficient accuracy will provide a benchmark for a fixed set of potentials.

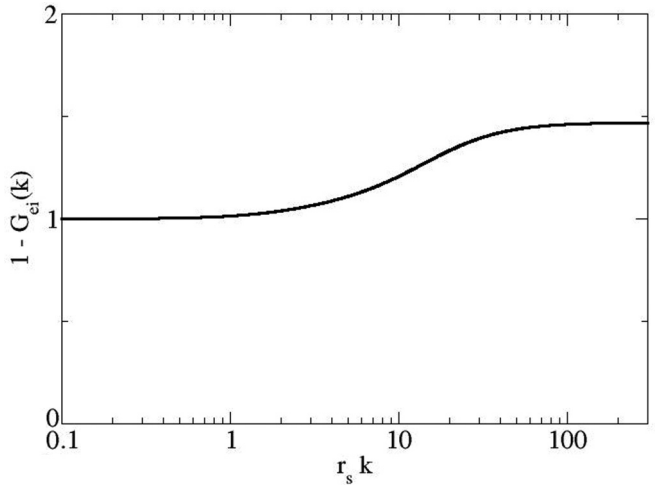

FIG. 8. $1 - G_{ei}(k)$ vs kr_S for $T_e = 1$ keV and $T_p = 0.8$ keV for H as calculated by HNC with the Dunn-Broyles potential.

Since LFCs are a result of many-body screening phenomena beyond the realm of RPA, it is reasonable to assume that their magnitudes should depend on density. We indeed find this to be the case. CS-GLB calculations of temperature equilibration on the $T_e = 1$ keV isotherm (with $T_p = 800eV$) are shown in Fig. 9. Dunn-Broyles potentials are used here. The differences between dT_e/dt with and without HNC-derived static LFCs decrease as n is decreased. Again, the no-LFC results have lower equilibration rates.

There are two possible reasons that CS-GLB with HNC-derived static $G_{ij}(k)$ is *less* accurate than CS-GLB with $G_{ij} = 0$. (1) The HNC approximation produces poor results for static correlations, in comparison to MD. This is checked by comparing the radial distribution functions, $g_{ij}(r)$ for HNC and MD for a given case, and for a given set of input potentials, $v_{ij}(k)$. (2) The *static* LFC assumption is inappropriate for these applications; that is, one needs $G_{ij}(k,\omega)$ rather than $G_{ij}(k)$. If HNC and MD $g_{ij}(r)$ agree, the static LFC assumption must be the culprit. Figure 10 shows HNC and MD $g_{ij}(r)$ results for a hydrogen plasma in equilibrium at $T = 1$ keV and $n = 10^{25}$/cc, for which the Dunn-Broyles + Deutch potentials have been used; they are nearly identical. In addition, we have demonstrated that the use of *equilibrium* HNC for our *non*-equilibrium situations does not alter our results for τ_{ei} by enough to warrant concern. Thus, we conclude that dynamical LFCs must play a role in determining the temperature relaxation of classical opposite-charge plasmas with Dunn-Broyles two-body interactions, and that the assumption of static LFCs for these plasmas leads to an overestimation of the impact of physics beyond the RPA.

Our initial interest in exploring the use of static LFCs in the GLB calculations comes from our reading of Ref. [10]. In this paper, the authors perform like-charge classical MD simulations of positrons and protons interacting via the pure Coulomb potential, which they analyze with GLB calculations. They show that in the absence of quantum diffraction, it is necessary to include LFCs in the GLB calculations to get

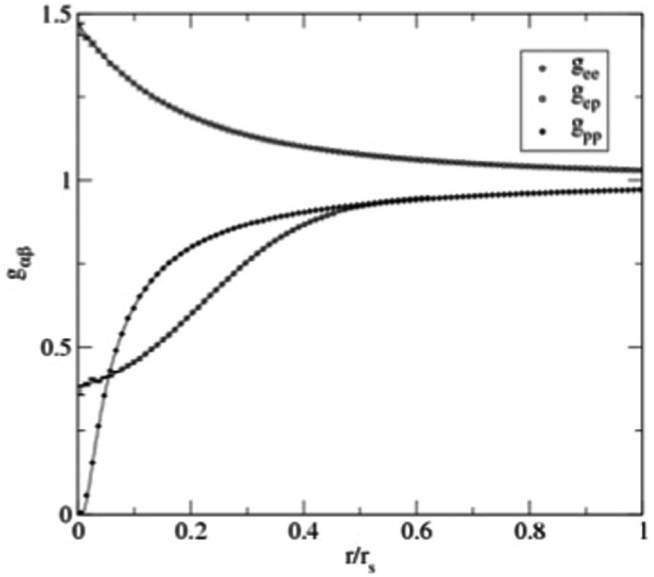

FIG. 10. Radial distribution functions, $g_{\alpha\beta}(r)$, for H at $n = 10^{25}$/cc and $T_e = T_p = 1$ keV. Both HNC (lines) and MD (points) results are shown, each using the Dunn-Broyles potential.

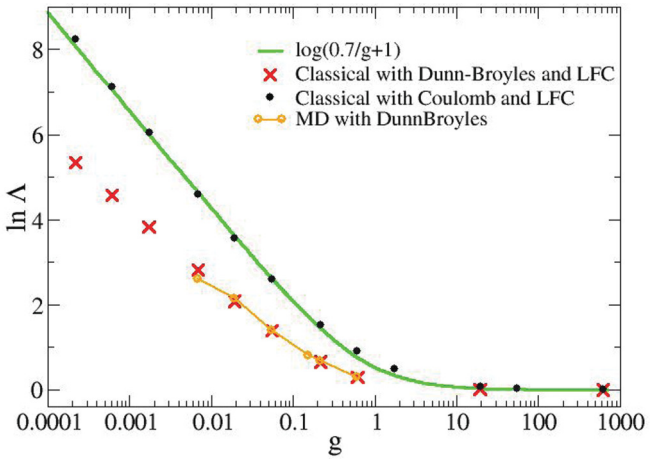

FIG. 12. (Color online) Effective $\ln \lambda_{ei}$ for the positron-proton system ($n = 10^{25}$/cc) vs the dimensionless plasma coupling, $g \equiv b_0/\lambda_{\text{Debye}}$. Results are from classical GLB with the Coulomb interaction (black points) and the Dunn-Broyles statistical potential (red points). The green curve is a fit to the MD results reported in Ref. [10].

a finite answer for the temperature relaxation rate for this system. Otherwise, the large-k part of $F(k) \longrightarrow 1/k$, and $\ln \lambda_{ei} = \int_0^\infty F(k)dk$ diverges. Furthermore, they argue that if static, HNC-derived $G_{ij}(k)$ are included for this system, the resulting $\ln \lambda_{ei}$ integral acquires the appropriate effective $b_{\min} \sim b_0 = e^2/k_B T_e$, the Landau length. This occurs because $1 - G_{ei}(k)$ goes to zero at roughly $k = 1/b_0$ (see Fig. 2 of Ref. [10]). In the end, their GLB results with these $G_{ij}(k)$ included agree very well with their like-charge pure-Coulomb MD. We have checked that our methodology to compute the static LFCs with HNC reproduces this result. Figure 11 shows plots of $1 - G_{ei}(k)$ vs $r_S.k$ for many temperatures and at a single density, $n = 10^{25}$/cc, for the classical pure-Coulomb positron-proton system. For each T_e, $1 - G_{ei}(k) = 1/2$ for $k \sim 1/b_0$. The resulting effective $\ln \lambda_{ei}$ for these cases, as calculated by CS-GLB, behaves as shown by the black dots in Fig. 12, here plotted against the dimensionless coupling

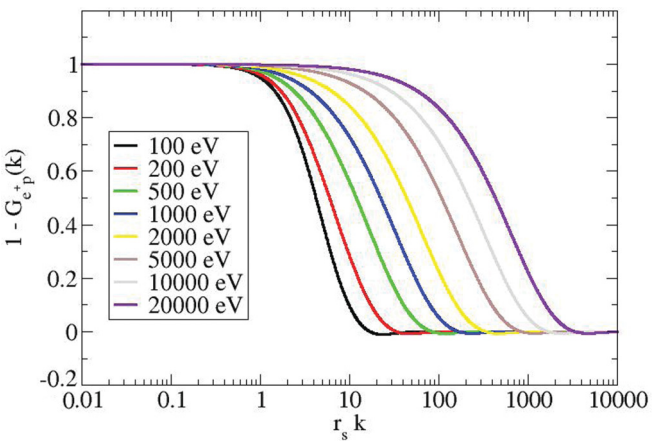

FIG. 11. (Color online) HNC results for $1 - G_{ei}(k)$ for the classical positron-proton system at $n = 10^{25}$/cc, performed with the pure Coulomb interaction.

$g \equiv b_0/\lambda_{\text{Debye}}$. This is essentially equivalent to Fig. 1 of Ref. [10], though we have extended to larger g by considering lower T.

Our opposite-charge studies with SPs suggest that the use of static LFCs produces worse results than if LFCs are set to zero, while like-charge pure-Coulomb studies show that they are necessary and lead to accurate results. This confusing state of affairs prompts us to consider the *like*-charge classical case *with the SPs*. The red crosses of Fig. 12 show the results of CS-GLB with the Dunn-Broyles potential for these same like-charge cases. Note that they lie well below the pure-Coulomb results for small g. This is because $\lambda_{\text{th}} > b_0$ for small g, and the softening of the potential at short-range produces an effective $b_{\min} \sim \lambda_{\text{th}}$. For $g = 19.37$, $\lambda_{\text{th}} \sim b_0$, and this is where the red and black symbols meet. The interesting case of g large enough so that $b_0 > \lambda_{\text{th}}$ is just to the right of the results in Fig. 12. These cases are likely not amenable to treatment with CS-GLB, since they are quite strongly coupled. More work must be done in the future to address the limits of GLB for like-charge systems such as these. For the more physically relevant opposite-charge cases at the equivalent couplings, the appearance of (classical) bound states would render GLB, as presented here and in Ref. [10], completely inadequate.

The conclusion for our hydrogen studies can be summarized simply: Comparison to GLB for weakly coupled cases shows that classical MD with Dunn-Broyles SPs should lead to electron-ion temperature equilibration rates which are roughly 10%–15% lower than the pure-Coulomb quantum answers in the fusion-burning regime ($n \sim 10^{25}$/cc, $T \sim$ a few keV). As the temperature is raised, the quantum answer is approached. The precise nature in which it is approached at high T is addressed in the Appendix. Statistical potentials based on the exact quantum pair density matrix (of the Kelbg variety) should lead to τ_{ei} which are far more accurate than those produced with Dunn-Broyles potentials. The use of classical HNC-derived static LFCs in the Lenard-Balescu calculations

does *not* lead to better agreement with classical MD for these opposite-charge cases where the SPs are used.

There are still some uncomfortable unknowns which await further study: We have no theory (analogous to GLB) which is expected to work at strong electron-ion coupling. As such, our ability to validate the MD with SPs is greatly hampered there. We have no rigorous means of estimating LFCs for the quantum case; thus, we do not know the extent to which our conclusions regarding the need for dynamic LFCs in the classical opposite-charge studies have any bearing for real quantum plasmas. Finally, preliminary results of ours suggest that plasmas for which the species have more similar masses may be less amenable to treatment with the GLB as presented here; MD results (Dunn-Broyles + Deutch SPs) for mass-scaled hydrogen with $n = 10^{25}$/cc, $T \sim 1$ keV, and $m_p = 10m_e$ relax a full 20% slower than the predictions of GLB for this same system, in contrast to the nice agreement shown in Fig. 3 for the physical mass case. Preliminary studies of this system with the Fokker-Planck equation suggest that this discrepancy is due to slight but important deviations of the velocity distributions from the Maxwellian forms assumed in our theoretical treatment [50].

One might argue that classical MD with SPs is not needed if one is simply interested in determining τ_{ei} for pure hydrogen in the fusion-burning regime, since weak-coupling theories such as the GLB and BPS can be used here instead. Indeed, it is because we are confident of the efficacy of GLB that we are able to "validate" the MD in the way that we have. The practical situation is more nuanced, however: As we mentioned in the Introduction, the real interest concerns H or DT plasmas mixed with higher-Z dopants. When a system such as this is driven out of equilibrium, the resulting temperature relaxation involves electrons scattering off protons, electrons scattering off the high-Z element, and proton-high-Z scattering as well. For many plasmas of interest, the $Z - Z$ coupling will be rather large. In this case, it is crucial to use a method of calculation which includes all possible many-body correlations in a time-dependent way, such as MD. The study presented above for pure H ensures that the electron-proton piece of this coupled-rate problem will be accurately evaluated. It is to a problem of this type that we now turn.

B. Ar-doped H

We consider a plasma consisting of hydrogen at a density of $n_H = n_p = n_e = 10^{25}$/cc, doped with 10 at.% argon. We choose the initial temperatures of the Ar ions and protons to be 6.6 keV, and the initial temperature of the electrons to be 4.5 keV. In these conditions, the Ar ions would be fully stripped ($Z_{\rm Ar} = +18$), so the species densities are $n_p = 10^{25}$/cc, $n_{\rm Ar} = 10^{24}$/cc, and $n_e = 2.8 \times 10^{25}$/cc. Our simulation cell contains 560 000 electrons, 200 000 protons, and 20 000 Ar^{18+} ions. We use the Dunn-Broyles potentials with the Deutch Pauli correction for this study, though the above analysis for H strongly suggests that Kelbg potentials would be better for reproducing the true quantum answer for at least the *ep* channel of the relaxation.

Using a standard three-species LS treatment for this system (see below), we find that τ_{ei} is of order 2000 fs. Given the small time steps required for an accurate rendering of the dynamics, we choose to perform the MD simulation with reduced ion masses: $m_p \longrightarrow \alpha m_p$, and $m_{\rm Ar} \longrightarrow \alpha m_{\rm Ar}$, where $\alpha = 0.01$. This trick has been used often for simulating two-species plasmas (for example, Ref. [21]) and three-species systems in which the ions have somewhat similar masses [23]. The idea is to take advantage of the fact that the primary dependence of the temporal evolution on the mass ratios is in the kinematic prefactor appearing, for instance, in Eq. (1). The dependencies within the Coulomb logarithms are often less important, though they are by no means negligible, as implied in the work of Ref. [23]. Considering only the mass dependence in the prefactor, the true relaxation can then be obtained by dividing the time scale by α.

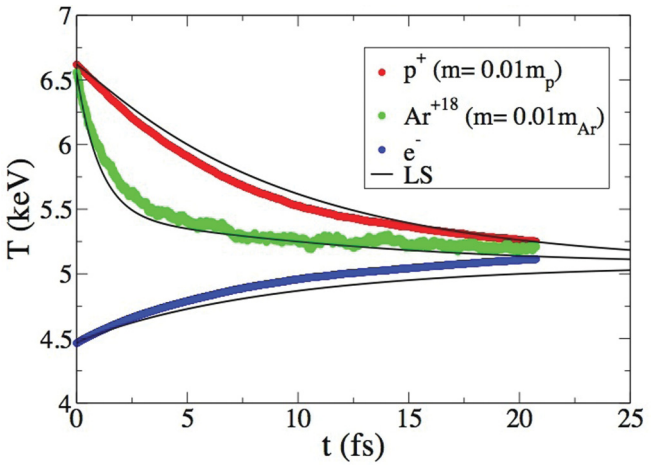

FIG. 13. (Color online) MD results (colored thick curves) and results of LS (black thin curves) for the scaled-mass ($\alpha = 0.01$) Ar-doped H plasma. Species densities are $n_p = 10^{25}$/cc, $n_{\rm Ar} = 10^{24}$/cc, and $n_e = 2.8 \times 10^{25}$/cc. $Z_{\rm Ar}$ is fixed at +18. MD was performed with the Dunn-Broyles potential, and the LS Coulomb logarithms were chosen according to the prescription outlined in Sec. 5.2 of Ref. [35].

Our MD results for this mass-scaled Ar-doped H plasma are shown in Fig. 13. The thick colored lines show the MD data, while the thin black lines show the results of LS with appropriately chosen Coulomb logarithms for each pair of species [35]. Several notable features should be mentioned. (1) The short time scale of the equilibration (tens of fs) is due to the mass scaling. If the time scale is multiplied by 100 (as per the aforementioned prescription), something akin to the physical temperature relaxation is recovered. (2) The final equilibrated temperature is closer to the initial temperature of the electrons than to that of the ions. This is simply because there are ~3 times as many electrons as ions, so the heat capacity of the electron subsystem is larger [23,24]. (3) The final equilibrated temperature is slightly higher than that predicted by LS. This is because the Ar-Ar coupling is somewhat high (because $Z_{\rm Ar} = 18$), so potential energy is substantively lowered in the final state in which the ions are colder- and kinetic energy must rise if the potential energy falls, as mandated by total energy conservation [23,24,35]. This is a subtle effect even for this case, in which 10 at.% of a fully stripped ion is present. We emphasize that it is beyond the scope of not only LS, but the GLB as well (as we have presented it here), since explicit potential energy contributions are absent

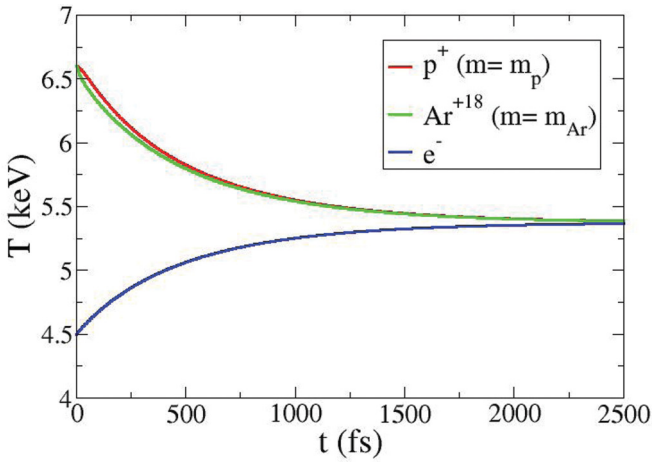

FIG. 14. (Color online) LS results for the physical-mass ($\alpha = 1$) Ar-doped H plasma with Coulomb logarithms all set to unity. Species densities are $n_p = 10^{25}$/cc, $n_{\rm Ar} = 10^{24}$/cc, and $n_e = 2.8 \times 10^{25}$/cc. $Z_{\rm Ar}$ is fixed at +18.

in, for instance, Eq. (19). Rigorous inclusion of potential energy effects within this context have recently appeared, however [11]. (4) The p and Ar temperatures, though chosen to be the same initially, quickly separate before coming together again at later times. This is due to the sizable difference in mass between p and Ar, the large $Z_{\rm Ar}$, and the fact that there are many more electrons than protons, which causes the Ar ions to be pulled toward the electrons more rapidly than the protons.

It would be tempting to conclude that the initial p-Ar temperature split is a robust result not only for the scaled-mass system, but for the corresponding plasma with physical p and Ar masses, once the time-scale is multiplied by $1/\alpha = 100$, since *both* m_p *and* $m_{\rm Ar}$ were scaled by the *same* factor. This, however, is not the case. Figure 14 shows simplified LS results for this system with $\alpha = 1$, in which all the Coulomb logarithms have been set to unity. Not only is the equilibration time greater by a factor of ∼100, as expected, but there is no sizable p-Ar temperature split. In contrast, Fig. 15 shows the

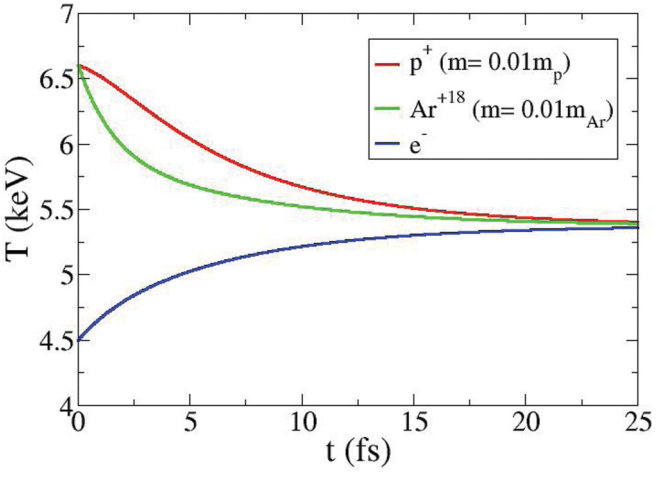

FIG. 15. (Color online) LS results for the scaled-mass ($\alpha = 0.01$) Ar-doped H plasma with Coulomb logarithms all set to unity. Species densities are: $n_p = 10^{25}$/cc, $n_{\rm Ar} = 10^{24}$/cc, and $n_e = 2.8 \times 10^{25}$/cc. $Z_{\rm Ar}$ is fixed at +18.

simplified $\ln \lambda_{ei} \equiv 1$ LS results for the $\alpha = 0.01$ system. The p-Ar temperature split is again apparent, as in Fig. 13. Thus, we see that the mass-scaling approach, while appropriate for many two-species problems, is highly suspect for the more complex case of multiple ion species. This is unfortunate, since it is in precisely these cases where it is often desirable to speed up the simulation. However, it is also reassuring that, at least for this particular Ar-doped H plasma, it might be possible to adopt a more coarse-grained approach in which the ions are lumped together into an "average ion." Such a simplified picture is often invoked in continuum simulations of multicomponent plasmas. It should be noted that in multi-ion plasmas where the ion masses are more similar, mass scaling may still be a useful construct [23].

We end our discussion of this mass-scaled Ar-doped H plasma by comparing to three-species GLB calculations. As for hydrogen, we use the GLB in three modes: QC-GLB with LFCs set to zero, CS-GLB with LFCs set to zero, and CS-GLB with static LFCs derived from HNC calculations. There are three couplings which must be computed in any given GLB calculation: ep, e-Ar, and p-Ar. For the p-Ar term, we include static HNC-derived LFCs, $G(k)$, for *each* of the different flavors of GLB we use. The reason for this is that the de Broglie wavelengths of the p and Ar are miniscule, owing to their large masses. Thus, for this coupling, the p-Ar Landau length is by far the dominant length-scale governing the small distance part of the Coulomb scattering. If we omitted the $G_{p-Ar}(k)$ here, the p-Ar term, analogous to the ei term of Eq. (20), would fail to converge at large k. The ep and e-Ar terms are treated, for each variant of GLB, in the manner described above for H.

The initial slopes of the species temperatures, as inferred from the MD data of Fig. 13, are listed in Table IV, along with the results of the three variants of GLB. As for hydrogen (see, e.g., the red curve of Fig. 3), the QC-GLB rates are larger than those of MD. The results of classical ($\hbar \longrightarrow 0$) GLB with LFCs set equal to zero are in somewhat better agreement with the MD, though the slope of the electron temperature is notably too small. Inclusion of HNC-derived LFCs for every pair of species leaves dT_p/dt and $dT_{\rm Ar}/dt$ relatively unchanged while raising dT_e/dt slightly toward the MD value. So we see again that the major effect of using classical MD with two-body SPs of the Dunn-Broyles variety is to lower the temperature equilibration rates relative to the predictions based on quantum dynamics and the pure Coulomb interaction.

V. CONCLUSIONS

We have used nonequilibrium classical MD with two-body SPs to simulate temperature equilibration in pure hydrogen and Ar-doped hydrogen plasmas. We discussed the way in which the two-temperature simulations are equilibrated, the method for extracting the relaxation times, issues of convergence (system size, time steps), and the SPs used. Results of the MD were found to be in accord with expectations gleaned from the LS theory, though a more quantitative understanding of these results was made possible by appealing to a many-body theory devoid of some of the approximations inherent in the LS treatment.

By performing generalized Lenard-Balescu calculations in both quantum and classical modes, it was shown that classical

MD with SPs should yield the quantum result in the limit of sufficiently weak coupling. This means that the salient features of quantum diffraction, crucial for the short-distance part of Coulomb scattering at high-temperatures, are captured in these approaches. However, our results also suggest that the specific potentials we used should give rise to temperature equilibration rates which are between a few percent and greater than 10% lower than those of the true quantum system in the fusion-burning regime. We demonstrated that SPs of the Kelbg variety, derived from the exact two-body thermal density matrix, are substantially better than Dunn-Broyles potentials, in that they reproduce the quantum pure-Coulomb result more accurately at all temperatures. Inclusion of static LFCs in the Lenard-Balescu calculations produced, for pure hydrogen, worse results, when comparing to the MD, than GLB calculations, which neglected LFCs altogether. This suggests that a full understanding of the classical *attractive*-potential temperature equilibration problem awaits the further study of dynamical LFCs. In this way, the work presented here serves to (1) better define the limits of applicability of quantum SPs in simulating dynamical phenomena and (2) clarify the limits of our understanding of the many-body phenomena important for the determination of temperature equilibration rates for hydrogen in the fusion burning regime.

Finally, study of a hydrogen plasma doped with fully stripped Ar demonstrated that mass scaling in the MD can be a dangerous proposition, while comparisons with GLB calculations reaffirm the above conclusions regarding both the utility and the limits of classical MD with SPs. It will be important and interesting in the future to direct attention to the significantly more complex problem of high-Z dopants which are not fully stripped during the course of temperature equilibration, as well as to electron-ion temperature equilibration in the presence of radiation.

ACKNOWLEDGMENTS

We thank R. M. More, J. C. Weisheit, F. H. Streitz, A. B. Langdon, R. A. London, J. Daligault, G. Dimonte, D. O. Gericke, R. E. Rudd, W. Mori, and S. D. Baalrud for helpful discussions. This work was performed under the auspices of the US Department of Energy at the Lawrence Livermore National Laboratory under Contract No. DE-AC52-07NA27344. This work was funded by the Laboratory Directed Research and Development Program at LLNL under tracking code No. 12-SI-005.

APPENDIX: CLASSICAL AND QUANTUM T-EQUILIBRATION RATES SHOULD APPROACH EACH OTHER AS $1/\ln(T)$

Here we show that the temperature equilibration rate computed classically with a SP (such as in the MD calculations we describe) should approach that of the true quantum rate as temperature is increased. We consider hydrogen at weak enough coupling so that the generalized Lenard-Balescu theory presented in Ref. [10] and discussed in Sec. III A is thought to be valid. Using this theory, we show that

$$\lim_{T\longrightarrow\infty}\left[\frac{\nu_{ie}(\mathrm{QC})-\nu_{ie}(\mathrm{SP})}{\nu_{ie}(\mathrm{QC})}\right]\propto\frac{1}{\ln(T)}, \tag{A1}$$

where $\nu_{ie}=1/\tau_{ie}$. QC indicates the quantum result with the pure Coulomb interaction, and SP indicates the classical ($\hbar\longrightarrow 0$) result with some set of SPs.

We make the following assumptions. (1) At the density we consider, the electron temperature, hereafter simply denoted T, is high enough so that the Debye screening length, λ_D, is much larger than the electron thermal de Broglie wavelength, λ_{th}. (2) $m_e T_{\mathrm{proton}}/m_{\mathrm{proton}}T\ll 1$; this is certainly satisfied for the physical mass ratio when, for instance, $T_{\mathrm{proton}}=0.8T$. It is then possible to simplify Eq. (20) by invoking the f-sum rule for the ions that eliminates the integral over ω [10]. (3) The density and temperature are such that the quantum electron distribution function is Maxwellian. (4) The Fourier transform of the SP is of the form

$$v_{ei}(k)=\frac{4\pi e^2}{k^2}K\left(\frac{k}{k_{\mathrm{th}}}\right), \tag{A2}$$

where $k_{\mathrm{th}}=1/\lambda_{\mathrm{th}}$ is the thermal de Broglie wave vector, and $K(x)=1$ for x much less than 1, while $K(x)\longrightarrow 0$ for x much greater than 1; this is satisfied, for instance, by the Dunn-Broyles and modified-Kelbg potentials we have used in this study.

If the plasma coupling is sufficiently weak, the thermal de Broglie wavelength is well above the Landau length and LFCs can be neglected. Thus, we set $G_{ei}=G_{ee}=G_{ii}=0$, and Eq. (20) plus the application of the ion f-sum rule leads to [10]

$$\nu_{ie}=-\frac{1}{3\pi^2 n_i}\int_0^\infty dk k^4\frac{|v_{ei}(k)|^2}{|\epsilon_e(k,0)|^2}\frac{\partial\chi_e^0(k,\omega=0)}{\partial\omega}, \tag{A3}$$

where $\epsilon_e(k,0)=1-v_{ee}(k)\chi_e^0(k,0)$. This expression applies for both classical-SP (SP) and quantum-Coulomb (QC) cases. We assume that the static electron dielectric function can be approximated by

$$\epsilon_e(k,0)=1+\frac{k_D^2}{k^2}, \tag{A4}$$

where $k_D=1/\lambda_D$ is the Debye screening wave vector. Though not exact, this approximate relation holds quite well for both SP and QC in the weak-coupling cases we consider. For QC, $v_{ei}(k)=4\pi e^2/k^2$, and [10]

$$\frac{\partial\chi_e^0(k,\omega=0)}{\partial\omega}=-\frac{n_e}{(k_BT)^{3/2}}\sqrt{\frac{\pi m_e}{2}}\frac{1}{k}f\left(\frac{k}{2}\right), \tag{A5}$$

where

$$f\left(\frac{k}{2}\right)=\frac{\frac{3\sqrt{\pi}}{4}\left(\frac{k_BT}{E_F}\right)^{3/2}}{1+\exp\left(\frac{\hbar^2k_F^2}{8m_ek_BT}\right)\exp(-\beta\mu)}. \tag{A6}$$

We here consider spinless electrons, so the E_F in the above numerator is $\hbar^2(6\pi^2n_e)^{2/3}/2m_e$. Furthermore, the assumption of Maxwellian electrons allows us to assert,

$$\exp(-\beta\mu)=\frac{1}{n_e\lambda_{\mathrm{th}}^3}=\frac{1}{n_e}\frac{(2\pi m_ek_BT)^{2/3}}{h^3}\gg 1. \tag{A7}$$

This gives us

$$\nu_{ie}(\mathrm{QC})=\frac{16e^4n_e}{3n_i(k_BT)^{3/2}}\sqrt{\frac{\pi m_e}{2}}\int_0^\infty\frac{dk}{k}\frac{\exp\left[-\frac{1}{16\pi}\left(\frac{k}{k_{\mathrm{th}}}\right)^2\right]}{\left(1+\frac{k_D^2}{k^2}\right)^2}. \tag{A8}$$

For SP, we take the interaction of Eq. (A2) and use the classical ($\hbar \longrightarrow 0$) result [10],

$$\frac{\partial \chi_e^0(k,\omega=0)}{\partial \omega} = -\frac{n_e}{(k_B T)^{3/2}}\sqrt{\frac{\pi m_e}{2}}\frac{1}{k}, \tag{A9}$$

which then yields

$$\nu_{ie}(\mathrm{SP}) = \frac{16e^4 n_e}{3n_i(k_B T)^{3/2}}\sqrt{\frac{\pi m_e}{2}}\int_0^\infty \frac{dk}{k}\frac{K^2\left(\frac{k}{k_{\mathrm{th}}}\right)}{\left(1+\frac{k_D^2}{k^2}\right)^2}. \tag{A10}$$

The only difference between $\nu_{ie}(\mathrm{QC})$ and $\nu_{ie}(\mathrm{SP})$ is the exponential factor in the former case and the $K^2(k/k_{\mathrm{th}})$ in the latter, both of which are functions of k/k_{th}. To simplify the equations that follow, we define the exponential factor in the QC case to be $H(k/k_{\mathrm{th}}) = \exp[-(1/16\pi)(k/k_{\mathrm{th}})^2]$, thereby exhibiting the formal similarity to the SP case,

$$\nu_{ie}(\mathrm{QC}) = \frac{16e^4 n_e}{3n_i(k_B T)^{3/2}}\sqrt{\frac{\pi m_e}{2}}\int_0^\infty \frac{dk}{k}\frac{H\left(\frac{k}{k_{\mathrm{th}}}\right)}{\left(1+\frac{k_D^2}{k^2}\right)^2}. \tag{A11}$$

Since both $K^2(x)$ and $H(x)$ approach 1 for x much less than 1, it is immediately apparent from Eqs. (A10) and (A11) that the k-integrands for SP and QC are identical for $k \ll k_{\mathrm{th}}$. This is shown in Fig. 16, in which the GLB integrands, multiplied by k, are plotted for SP (Dunn-Broyles potentials are used here) and QC for hydrogen with $n = 10^{25}$/cc, $T_e = 100\,000$ eV, and $T_p = 80\,000$ eV. In such a weakly coupled case, there is a large range of k where the integrands divided by the LS prefactor, denoted $F(k)$ as in the main text, are equal to $1/k$; this is the range $k_D < k < k_{\mathrm{th}}$. In order to estimate the T dependence of these integrals, we break them into three distinct regions, also indicated in Fig. 16 [we define $F(k)$ to be the integrands appearing in Eqs. (A10) and (A11), excluding the common prefactors to the left of the integral signs]:

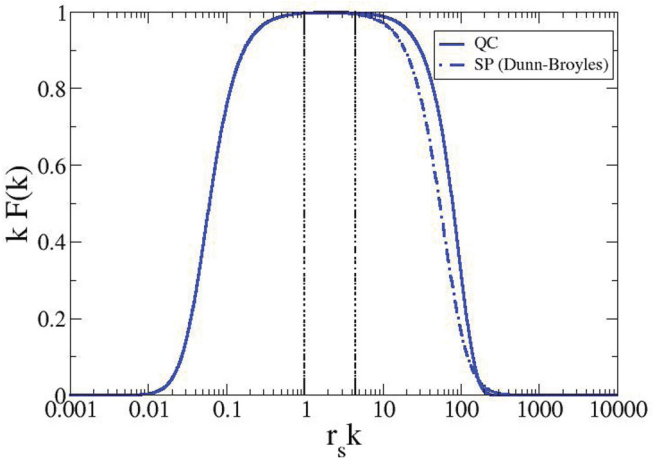

FIG. 16. (Color online) The GLB k-integrand divided by the LS prefactor, $F(k)$, multiplied by k for both QC and SP (Dunn-Broyles) cases for hydrogen at $n = 10^{25}$/cc, $T \equiv T_e = 100\,000$ eV, and $T_p = 0.8T_e$. The vertical dotted lines are located at $k = ak_D$ and bk_{th}, respectively, and define low-k, middle-k, and high-k regions (see text). Between the dotted lines, $F(k) \sim 1/k$. As T is increased further, the middle-k region expands at the expense of the outer regions. QC and SP $F(k)$ only differ in the high-k region.

$$\frac{\nu_{ie}}{P} = \int_0^{ak_D} dk F(k) + \int_{ak_D}^{bk_{\mathrm{th}}} dk F(k) + \int_{bk_{\mathrm{th}}}^\infty dk F(k), \tag{A12}$$

with

$$P = \frac{16e^4 n_e}{3n_i(k_B T)^{3/2}}\sqrt{\frac{\pi m_e}{2}}.$$

In Eq. (A12), a is larger than 1 and b is less than 1, ensuring that the middle region (see Fig. 16) defines a range in which $F(k) \sim 1/k$. Clearly, both the low-k and middle-k pieces of Eq. (A12) will be equal for QC and SP cases, so $\nu_{ie}(\mathrm{QC}) - \nu_{ie}(\mathrm{SP})$ is completely determined by the differences in their high-k pieces. We have

$$\int_{bk_{\mathrm{th}}}^\infty dk F(k) = \int_{bk_{\mathrm{th}}}^\infty \frac{dk}{k} Q\left(\frac{k}{k_{\mathrm{th}}}\right) = \int_b^\infty \frac{dx}{x} Q(x) \equiv I_{\mathrm{th}}(b), \tag{A13}$$

where Q denotes either H (QC) or K^2 (SP). Since b is a constant independent of T, we have demonstrated that $\nu_{ie}(\mathrm{QC}) - \nu_{ie}(\mathrm{SP}) \propto T^{-3/2}$, which is not surprising given the T dependence of the LS prefactor shown in Eq. (1). The factor multiplying $T^{-3/2}$ in this difference is determined by the prefactor shown in Eqs. (A10) and (A11), as well as by the difference between the QC and SP integrals represented in Eq. (A13), $I_{\mathrm{th}}^{\mathrm{QC}}(b) - I_{\mathrm{th}}^{\mathrm{SP}}(b)$.

In order to form the quotient of Eq. (A1), we must estimate the rest of the integral as well, which is equal for SP and QC. For the low-k piece, we have

$$\int_0^{ak_D} dk F(k) = \int_0^{ak_D} \frac{dk}{k\left(1+\frac{k_D^2}{k^2}\right)^2} = \int_0^a \frac{dx}{x\left(1+\frac{1}{x^2}\right)^2} \equiv I_D(a). \tag{A14}$$

For the intermediate-k piece, we have simply

$$\int_{ak_D}^{bk_{\mathrm{th}}} dk F(k) = \int_{ak_D}^{bk_{\mathrm{th}}} \frac{dk}{k} = \ln\left(\frac{bk_{\mathrm{th}}}{ak_D}\right) = [\ln(T) + A], \tag{A15}$$

where A is a constant; here we have used the fact that $k_{\mathrm{th}}/k_D \propto T$. Combining all the pieces gives

$$\frac{\nu_{ie}(\mathrm{QC}) - \nu_{ie}(\mathrm{SP})}{\nu_{ie}(\mathrm{QC})} = \frac{I_{\mathrm{th}}^{\mathrm{QC}}(b) - I_{\mathrm{th}}^{\mathrm{SP}}(b)}{I_D(a) + \ln(T) + A + I_{\mathrm{th}}^{\mathrm{QC}}(b)}, \tag{A16}$$

which approaches $1/\ln(T)$ as $T \longrightarrow \infty$. Figure 17 shows the GLB (LFCs set to zero) predictions for the fractional differences in QC and SP equilibration rates on the $n = 10^{25}$/cc isochore, plotted in such a way as to exhibit the approach to this $1/\ln(T)$ behavior at high-T.

The main point is that weak plasma coupling guarantees that the differences between quantum and classical energy transfer rates are confined to large k as long as the SP used in the classical calculation is Coulombic for large separations

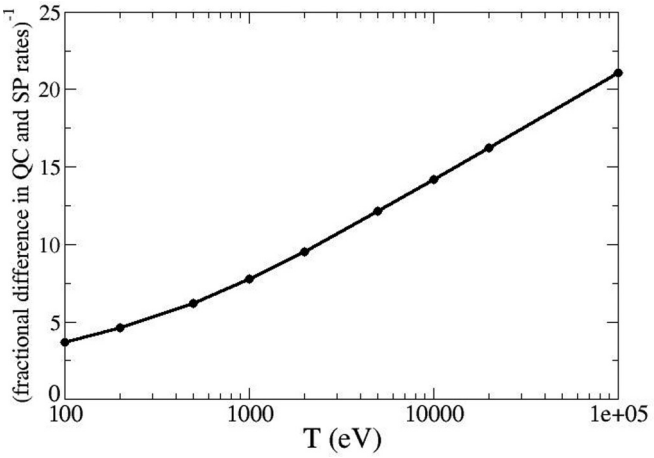

FIG. 17. The reciprocal of the fractional difference between QC and SP (Dunn-Broyles) rates, $\nu_{ie}(\mathrm{QC})/[\nu_{ie}(\mathrm{QC}) - \nu_{ie}(\mathrm{SP})]$, as a function of $T = T_e$ for the $n = 10^{25}$/cc isochore of hydrogen as computed by GLB (LFCs = 0). The semilog plot is linear for high T, indicating that the reciprocal of the fractional difference asymptotes to $\ln(T)$.

and is regularized at small separations within a thermal de Broglie wavelength. These differences depend on the precise form of the SP; we have seen in Sec. IV A that they are smaller for modified-Kelbg than for Dunn-Broyles, for instance. Yet since these large-k quantum and classical portions are both proportional to $T^{-3/2}$, the T dependence of the magnitude of the *fractional* differences in the rates is governed by the large intermediate-k piece which is common to both. This fractional difference is then nothing more than the Coulomb logarithm itself, $\ln\lambda_{ei} = \ln(\lambda_D/\lambda_{\mathrm{th}}) = \ln(k_{\mathrm{th}}/k_D) = \ln(T) + \mathrm{const}$.

Finally, we note that for plasmas satisfying the various criteria outlined at the start of this section (sufficiently weak coupling, large ep mass ratio for similar temperatures, etc.) it is possible to define a statistical potential for which a classical simulation of T equilibration should return the *exact* quantum answer: Examination of Eqs. (A8) and (A10) reveals that $\nu_{ie}(\mathrm{QC}) = \nu_{ie}(\mathrm{SP})$ if we choose

$$K\left(\frac{k}{k_{\mathrm{th}}}\right) = \exp\left[-\frac{1}{32\pi}\left(\frac{k}{k_{\mathrm{th}}}\right)^2\right]. \tag{A17}$$

It is doubtful, however, that the resulting ei potential,

$$v_{ei}(k) = -\frac{4\pi e^2}{k^2}\exp\left[-\frac{1}{32\pi}\left(\frac{k}{k_{\mathrm{th}}}\right)^2\right], \tag{A18}$$

would be in any way appropriate to use for reproducing the correct *static* properties of the quantum plasma, such as $g_{ei}(r)$, for instance. Optimization of such static properties is precisely what was used to derive the SPs we have used in this work (Dunn-Broyles, modified-Kelbg).

[1] E. I. Moses, R. N. Boyd, B. A. Remington, C. J. Keane, and R. Al-Ayat, Phys. Plasmas **16**, 041006 (2009).

[2] S. Azteni and J. Meyer-ter-Vehn, *The Physics of Inertial Fusion* (Clarendon Press, Oxford, 2004).

[3] B. Xu and S. X. Hu, Phys. Rev. E **84**, 016408 (2011).

[4] L. D. Landau, Phys. Z. Sowjetunion **10**, 154 (1936); Zh. Eksp. Teor. Fiz. **7**, 203 (1937); L. Spitzer, Jr., *Physics of Fully Ionized Gases*, 2nd ed. (Interscience, New York, 1962).

[5] We define the plasma coupling parameter for species i and j to be $\Gamma_{ij} = Z_i Z_j e^2/R_{ij}k_B T$, where R_{ij} is the average of the Wigner-Seitz ion sphere radii for species i and j.

[6] A recent work somewhat intermediate between that of LS and a full-blown many-body treatment appears in S. D. Baalrud, Phys. Plasmas **19**, 030701 (2012). Here, the binary collision approximation is made for particles interacting via a Debye-screened potential, and symmetry properties of the two-body collision operator are exploited, allowing for the study of large-angle scattering which occurs in more strongly-coupled plasmas.

[7] M. W. C. Dharma-wardana and F. Perrot, Phys. Rev. E **58**, 3705 (1998).

[8] L. S. Brown, D. L. Preston, and R. L. Singleton, Jr., Phys. Rep. **410**, 237 (2005).

[9] D. O. Gericke, M. S. Murillo, and M. Schlanges, Phys. Rev. E **65**, 036418 (2002).

[10] J. Daligault and G. Dimonte, Phys. Rev. E **79**, 056403 (2009).

[11] J. Vorberger, D. O. Gericke, Th. Bornath, and M. Schlanges, Phys. Rev. E **81**, 046404 (2010).

[12] J. P. Hansen and I. R. McDonald, Phys. Lett. A **97**, 42 (1983).

[13] E. H. Lieb, Bull. Am. Math. Soc. **22**, 1 (1990).

[14] P. Hohenberg and W. Kohn, Phys. Rev. **136**, B864 (1964); W. Kohn and L. J. Sham, *ibid.* **140**, A1133 (1965).

[15] D. M. Ceperley, in *Monte Carlo and Molecular Dynamics of Condensed Matter Systems*, edited by K. Binder and G. Ciccotti (Editrice Compositori, Bologna, Italy, 1996).

[16] R. Kosloff, Annu. Rev. Phys. Chem. **45**, 145 (1994).

[17] G. Dimonte and J. Daligault, Phys. Rev. Lett. **101**, 135001 (2008).

[18] T. Dunn and A. A. Broyles, Phys. Rev. **157**, 156 (1967).

[19] H. Minoo, M. M. Gombert, and C. Deutsch, Phys. Rev. A **23**, 924 (1981).

[20] G. Kelbg, Ann. Phys. **12**, 219 (1963).

[21] B. Jeon, M. Foster, J. Colgan, G. Csanak, J. D. Kress, L. A. Collins, and N. Gronbech-Jensen, Phys. Rev. E **78**, 036403 (2008).

[22] J. N. Glosli, F. R. Graziani, R. M. More, M. S. Murillo, F. H. Streitz, M. P. Surh, L. X. Benedict, S. Hau-Riege, A. B. Langdon, and R. A. London, Phys. Rev. E **78**, 025401(R) (2008).

[23] L. X. Benedict, J. N. Glosli, D. F. Richards, F. H. Streitz, S. P. Hau-Riege, R. A. London, F. R. Graziani, M. S. Murillo, and J. F. Benage, Phys. Rev. Lett. **102**, 205004 (2009).

[24] D. O. Gericke, J. Phys.: Conf. Ser. **11**, 111 (2005).

[25] S. X. Hu, B. Militzer, V. N. Goncharov, and S. Skupsky, Phys. Rev. Lett. **104**, 235003 (2010).

[26] F. H. Streitz, J. N. Glosli, and M. V. Patel, Phys. Rev. Lett. **96**, 225701 (2006).

[27] R. W. Hockney and J. W. Eastwood, *Computer Simulations Using Particles* (Adam Hilger, Bristol, UK, 1988).

[28] F. Reif, *Fundamentals of Statistical and Thermal Physics* (Waveland Press, Long Grove, 2008).

[29] J. P. Hansen and I. R. McDonald, Phys. Rev. A **23**, 2041 (1981).
[30] J. P. Hansen and I. R. McDonald, *Theory of Simple Liquids* (Elsevier, Amsterdam, 2006).
[31] J. P. Hansen, G. M. Torrie, and P. Vieillefosse, Phys. Rev. A **16**, 2153 (1977).
[32] B. Bernu and J. P. Hansen, Phys. Rev. Lett. **48**, 1375 (1982).
[33] A. V. Filinov, M. Bonitz, and W. Ebeling, J. Phys. A **36**, 5957 (2002).
[34] A. V. Filinov, V. O. Golubnychiy, M. Bonitz, W. Ebeling, and J. W. Dufty, Phys. Rev. E **70**, 046411 (2004).
[35] F. R. Graziani *et al.*, High Energy Density Phys. **8**, 105 (2012).
[36] H. D. Whitley *et al.* (unpublished).
[37] C. Deutsch, M. M. Gombert, and H. Minoo, Phys. Lett. A **66**, 381 (1978).
[38] C. Deutsch, M. M. Gombert, and H. Minoo, Phys. Lett. A **72**, 481 (1979).
[39] S. Ichimaru, *Statistical Plasma Physics, Vol. 1: Basic Principles* (Addison-Wesley, Redwood City, CA, 1992).
[40] The prefactor appearing in Eq. (12) is not the same as that shown in Eq. (4) of Ref. [10]. Though we follow their logic leading up to that equation, our definitions for the Fourier transforms of the fluctuating densities require the prefactor appearing here in order that we ultimately obtain the prefactors in our Eqs. (19) and (20), which correspond precisely to theirs in Eq. (10) (of Ref. [10]). It is on those final expressions, in terms of the free-particle susceptibilities, that we base our numerical evaluations of dT_α/dt.
[41] A. Fetter and J. D. Walecka, *Quantum Theory of Many Particle Systems* (McGraw-Hill, San Francisco, 1971).
[42] J. Chihara, J. Phys.: Condens. Matter **3**, 8715 (1991).
[43] R. G. Dandrea, N. W. Ashcroft, and A. E. Carlsson, Phys. Rev. B **34**, 2097 (1986).
[44] C. S. Jones and M. S. Murillo, High Energy Density Phys. **3**, 379 (2007).
[45] M. W. C. Dharma-wardana and M. S. Murillo, Phys. Rev. E **77**, 026401 (2008).
[46] J. F. Springer, M. A. Pokrant, and F. A. Stevens, J. Chem. Phys. **58**, 4863 (1973).
[47] K.-C. Ng, J. Chem. Phys. **61**, 2680 (1974).
[48] Y. Saad, *Iterative Methods for Sparse Linear Systems*, 2nd ed. (Society for Industrial and Applied Mathematics, Philadelphia, 2003).
[49] Note that the MD results for $T_e = 2$ and 5 keV fall slightly below the green curve (classical GLB [$G = 0$]). This is quite possibly a result of lack of convergence of the MD simulations with respect to time step. Though we attempted to use time steps that were sufficient for our desired accuracy (we used $\sim$ few $\times$ 10^{-6} fs for these), the exceedingly long simulation times for these weakly coupled cases precluded us from demonstrating time step convergence in a truly convincing way. We note further that our experience has shown us that when the time steps are not sufficiently small, the temperature equilibration rates are too low. We are currently implementing an advanced integration scheme that should allow us to address these more weakly coupled cases with higher fidelity.
[50] Here we used the Fokker-Planck scheme (though without DT burning) as outlined in D. Michta, F. Graziani, T. Luu, and J. Pruett, Phys. Plasmas **17**, 012707 (2010), with Coulomb logarithms appropriate for this case. Comparisons between Fokker-Planck and a LS treatment using identical Coulomb logarithms (which is simply Fokker-Planck but with particle distributions constrained to be Maxwellian) showed the same 20% reduction in the temperature equilibration rate. Non-Maxwellian behavior is to be expected here, simply because a small mass ratio implies that τ_{ee} and τ_{pp} are not necessarily much smaller than τ_{ep}. We also note that agreement between MD and GLB for these aggressively mass-scaled cases is recovered (for $n = 10^{25}$/cc) when T is as high as 20 keV, so the size of the plasma coupling is also possibly a factor.